Swarthmore College

Works

3-1-2024

Dynamical Architectures Of S-Type Transiting Planets In Binaries. I. Target Selection Using Hipparcos And Gaia Proper Motion Anomalies

J. Zhang

L. M. Weiss

D. Huber

See next page for additional authors

Follow this and additional works at: https://works.swarthmore.edu/fac-physics

Part of the Physics Commons

Let us know how access to these works benefits you

Recommended Citation

Authors

J. Zhang, L. M. Weiss, D. Huber, Eric L.N. Jensen, T. D. Brandt, K. Collins, D. M. Conti, H. Isaacson, P. Lewin, G. Marino, B. Massey, F. Murgas, E. Palle, D. J. Radford, H. M. Relles, G. Srdoc, C. Stockdale, T.-G. Tan, and G. Wang

Dynamical Architectures of S-type Transiting Planets in Binaries. I. Target Selection Using Hipparcos and Gaia Proper Motion Anomalies[*]

Jingwen Zhang (张婧雯)[1,20] [iD], Lauren M. Weiss[2] [iD], Daniel Huber[1] [iD], Eric L. N. Jensen[3] [iD], Timothy D. Brandt[4] [iD],
Karen Collins[5] [iD], Dennis M. Conti[6] [iD], Howard Isaacson[7,8] [iD], Pablo Lewin[9] [iD], Giuseppe Marino[10,11] [iD], Bob Massey[12] [iD],
Felipe Murgas[13,14] [iD], Enric Palle[13,14] [iD], Don J. Radford[15] [iD], Howard M. Relles[5], Gregor Srdoc[16], Chris Stockdale[17] [iD],
Thiam-Guan Tan[18] [iD], and Gavin Wang[19] [iD]

[1] Institute for Astronomy, University of Hawai'i, Honolulu, HI 96822, USA; jingwen7@hawaii.edu
[2] Department of Physics, University of Notre Dame 334 Nieuwland Science Hall, Notre Dame, IN 46556, USA
[3] Department of Physics & Astronomy, Swarthmore College, Swarthmore, PA 19081, USA
[4] Department of Physics, University of CaliforniaSanta Barbara, Santa Barbara, CA 93106, USA
[5] Center for Astrophysics | Harvard & Smithsonian, 60 Garden Street, Cambridge, MA 02138, USA
[6] American Association of Variable Star Observers, 185 Alewife Brook Parkway, Suite 410, Cambridge, MA 02138, USA
[7] 501 Campbell Hall, University of California Berkeley, Berkeley, CA 94720, USA
[8] Centre for Astrophysics, University of Southern Queensland, Toowoomba, QLD, Australia
[9] The Maury Lewin Astronomical Observatory, Glendora, CA 91741. USA
[10] Wild Boar Remote Observatory, San Casciano in val di Pesa, Firenze, I-50026 Italy
[11] Gruppo Astrofili Catanesi, Catania, Italy
[12] Villa '39 Observatory, Landers, CA 92285, USA
[13] Instituto de Astrofísica de Canarias (IAC), E-38205 La Laguna, Tenerife, Spain
[14] Departamento de Astrofísica, Universidad de La Laguna (ULL), E-38206 La Laguna, Tenerife, Spain
[15] American Association of Variable Star Observers, 49 Bay State Road, Cambridge, MA 02138, USA
[16] Kotizarovci Observatory, Sarsoni 90, 51216 Viskovo, Croatia
[17] Hazelwood Observatory,Churchill, Victoria, Australia
[18] Perth Exoplanet Survey Telescope, Perth, Western Australia, Australia
[19] Tsinghua International School, Beijing 100084, People's Republic of China

Abstract

The effect of stellar multiplicity on planetary architecture and orbital dynamics provides an important context for exoplanet demographics. We present a volume-limited catalog of up to 300 pc of 66 stars hosting planets and planet candidates from Kepler, K2, and TESS with significant Hipparcos-Gaia proper motion anomalies, which indicates the presence of companions. We assess the reliability of each transiting planet candidate using ground-based follow-up observations, and find that the TESS Objects of Interest (TOIs) with significant proper anomalies show nearly four times more false positives due to eclipsing binaries compared to TOIs with marginal proper anomalies. In addition, we find tentative evidence that orbital periods of planets orbiting TOIs with significant proper anomalies are shorter than those orbiting TOIs without significant proper anomalies, consistent with the scenario that stellar companions can truncate planet-forming disks. Furthermore, TOIs with significant proper anomalies exhibit lower Gaia differential velocities in comparison to field stars with significant proper anomalies, suggesting that planets are more likely to form in binary systems with low-mass substellar companions or stellar companions at wider separation. Finally, we characterize the three-dimensional architecture of LTT 1445 ABC using radial velocities, absolute astrometry from Gaia and Hipparcos, and relative astrometry from imaging. Our analysis reveals that LTT 1445 is a nearly flat system, with a mutual inclination of $\sim2°.88$ between the orbit of BC around A and that of C around B. This coplanarity may explain why multiple planets around LTT 1445 A survive in the dynamically hostile environments of this system.

Unified Astronomy Thesaurus concepts: Exoplanet catalogs (488); Exoplanet dynamics (490); Astrometric binary stars (79); Gaia (2360); Radial velocity (1332)

Supporting material: machine-readable tables

1. Introduction

Radial velocity (RV; Cumming et al. 2008; Fulton et al. 2021) surveys and space-based transit searches, such as Kepler (Borucki et al. 2010; Howard et al. 2012) and TESS (Ricker et al. 2014), have revolutionized our understanding of exoplanet demographics. However, the process of confirming exoplanets is biased against stars in multiple systems since close companions complicate the observations and analysis. Although one-third of nearby solar-type stars have at least one companion (Raghavan et al. 2010), the effects of stellar multiplicity on planetary architecture and orbital dynamics are still poorly understood. In addition, unknown stellar companions can cause inaccuracy in estimating planet radius by diluting the measured transit depths (Furlan et al. 2017; Teske et al. 2018; Sullivan et al. 2023). Planet properties may also be inaccurate if the planet is actually orbiting the secondary star. Thus, identifying the stellar companions of transiting planets helps obtain

---

more accurate planet parameters and characterize the demographics of planets in binaries (Fontanive & Bardalez Gagliuffi 2021; Cadman et al. 2022). By analyzing large samples of planets in binaries and comparing them to single systems, we can gain insights into the factors that shape the formation and evolution of exoplanets.

Close companions are expected to have a deleterious influence on planet formation, through disk truncation (Artymowicz & Lubow 1994; Jang-Condell et al. 2015) or dynamic stirring of planetesimals (Quintana et al. 2007). Recent Atacama Large Millimeter/submillimeter Array (ALMA) observations show that disks in binaries have lower masses (Akeson et al. 2019) and smaller radii (Cox et al. 2017; Manara et al. 2019), supporting the disk truncation scenario. Kraus et al. (2016) used high-resolution adaptive optics (AO) imaging of 382 Kepler Objects of Interest (KOIs) to show that the planet occurrence rate in close binaries (<47 au) is only 0.34 times that of single stars or wide binaries. Ziegler et al. (2020, 2021), Howell et al. (2021), Lester et al. (2021), and Ziegler et al. (2021) performed similar searches for stellar companions to TESS Objects of Interest (TOIs) and also found a deficit of close binaries (<100 au). For giant planets discovered by RV observations, Hirsch et al. (2021) reported that the planet occurrence rate in binaries with a separation <100 au is significantly smaller than those in binaries with a separation >100 au or single stars. Additionally, Fontanive & Bardalez Gagliuffi (2021) present a volume-limited sample of companions from tens of AU out to 20,000 AU in the literature and Gaia DR2 to exoplanet host stars. They found giant planets with masses above 0.1 M_J are more frequently seen than small sub-Jovian planets in binary systems, which is supported by the simulations by Cadman et al. (2022).

However, some planets survive in such dynamically challenging environments for reasons that are still unclear (Hatzes et al. 2003; Correia et al. 2008; Kane et al. 2015; Dupuy et al. 2016). Close binary companions could induce gravitational perturbations on their orbits, causing the migration or spin–orbit misalignment of planets. Furthermore, close companions may torque the proto-planetary disks where planets form, and therefore shape the architecture of the planet systems. Studying the architecture of planets in close binary systems will shed light on the planet formation and evolution of these systems.

Transit surveys, including TESS, Kepler, and K2, offer an unbiased planet sample in terms of stellar multiplicity. The coarse spatial resolution of TESS (21″ pixel^{-1}) and Kepler (4″ pixel^{-1}) makes it essential to conduct ground-based follow-up observations to resolve close binary systems. Previous studies have used adaptive optics (AO) and speckle imaging to search for stellar companions to planet candidate (PC) hosts discovered by Kepler and TESS missions (Kraus et al. 2016; Ziegler et al. 2020; Howell et al. 2021; Lester et al. 2021; Ziegler et al. 2021). The Gaia mission's renormalized unit weight error (RUWE) is also an indicator for companions, as RUWE values are sensitive to the deviation from the single-star astrometric model. However, RUWE values are most effective for detecting binaries with separations from 0″1–0″6 (Lindegren et al. 2018; Ziegler et al. 2020). The companions located outside of the range might be overlooked.

In this paper, we use Gaia (Gaia Collaboration et al. 2022) and Hipparcos (ESA 1997) proper motion anomalies (Brandt et al. 2019; Kervella et al. 2019) to identify close companions hiding in the large pixels of TESS or Kepler. The method takes

advantage of ~25 yr time baseline between the two missions, and is sensitive to companions with orbital periods from decades to centuries (Kervella et al. 2019). Furthermore, the combination of Gaia and Hipparcos astrometry, radial velocities (RVs), and imaging astrometry makes it possible to determine the 3D orbits of the companions and obtain their dynamical masses (Brandt et al. 2019; Xuan & Wyatt 2020). In this paper, we characterized the 3D orbits of companions in the proof-of-concept system LTT 1445 ABC with the method. It is important to note that our emphasis here is on the orbit parameters of stellar companions with orbital periods in years, rather than on transiting planets with much shorter orbital periods in the order of days. Finally, by obtaining the inclinations of the companion orbits, we can constrain the mutual inclinations between the orbital plane of the companion and that of the transiting planet. This information can provide insight into the system's dynamic history.

2. Hipparcos-Gaia Proper Motion Anomalies

The Gaia spacecraft (Gaia Collaboration et al. 2022) has measured the position and proper motion of nearly 1.7 billion stars since 2014. Its predecessor Hipparcos (Perryman et al. 1997) also provides precise astrometric measurements of nearby stars from 1989–1993. The measurements have a time baseline of nearly 25 yr and can detect the effect of unresolved binaries since a companion would cause the primary to wobble around the barycenter on the sky plane (Brandt et al. 2019; Kervella et al. 2019). Specifically, we use Hipparcos and Gaia EDR3 proper motions and their uncertainties from the Hipparcos-Gaia Catalog of Accelerations (HGCA; Brandt 2021). The catalog provides three proper motions for every star: (1) the Hipparcos proper motion μ_H at an epoch near 1991.25; (2) the Gaia EDR3 proper motion μ_G at an epoch near 2016.01; and (3) long-term proper motion μ_{HG} given by position difference between Hipparcos and Gaia divided by the 25 yr baseline.

These proper motions are in the unit of millarcsecond per year (mas yr^{-1}). The proper motions are given in R.A. (R.A., α) and decl. (decl., δ) direction. For simplicity, we use the total proper motion combined from the two directions and omit the subscript for R.A. and decl. in this paper. The long-term proper motion μ_{HG} can be used to estimate the velocity of celestial linear motion across the sky plane over nearly 25 yr. We subtracted the long-term proper motion μ_{HG} from Hipparcos and Gaia proper motions as follows:

$$\Delta\mu_H = \mu_H - \mu_{HG}$$
$$\Delta\mu_G = \mu_G - \mu_{HG}. \tag{1}$$

The two residuals represent the proper motion anomalies at the Hipparcos and Gaia epochs, respectively (Kervella et al. 2019). Note that these anomalies are also known as astrometric accelerations (Brandt 2021). We use the terminology of *proper motion anomalies* to prevent confusion with the general concept of *acceleration*, as the residuals are measured in the unit of mas yr^{-1}.

As shown in Figure 1, a significant proper motion anomaly reveals a deviation from the linear stellar motion, possibly caused by a gravitationally bound companion. We calculate the signal-to-noise ratio (S/N) of proper motion anomalies at Hipparcos and Gaia epochs using the calibrated uncertainties of
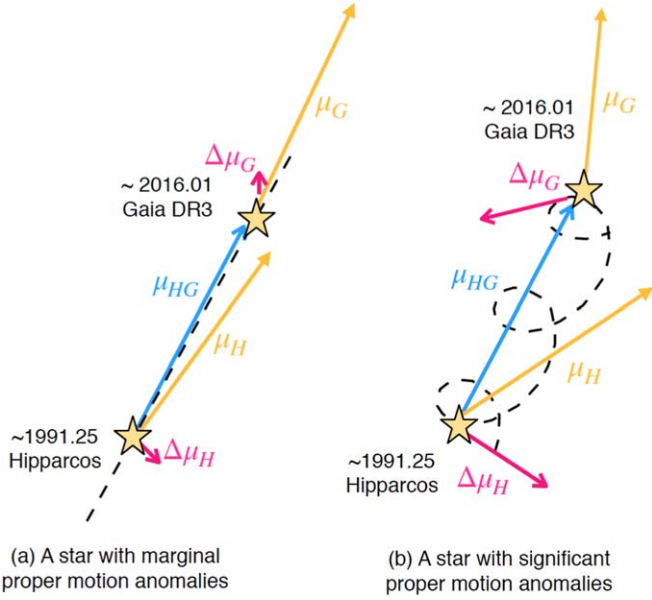
Figure 1. Principle of Hipparcos-Gaia proper motion anomalies. μ_H and μ_G represent the proper motions of the same star measured by Hipparcos and Gaia with a time baseline of around 25 yr. μ_{HG} is the stellar long-term velocity across the sky plane. If we subtract μ_{HG} from μ_H and μ_G, the residuals are the proper motion anomalies at the Hipparcos and Gaia epochs, respectively. (a) A star with marginal proper motion anomalies: if μ_H and μ_G are similar to the long-term velocity μ_{HG}, the star moves across the sky plane in a linear motion. (b) A star with significant proper motion anomalies: a significant residual indicates the star not only moves linearly but also orbits around the system's barycenter due to the gravitational pull from a companion.

Hipparcos and Gaia measurements from Brandt (2021):

$$S/N_G = \frac{\mu_G - \mu_{HG}}{\sqrt{\sigma[\mu_G]^2 + \sigma[\mu_{HG}]^2}}$$

$$S/N_H = \frac{\mu_H - \mu_{HG}}{\sqrt{\sigma[\mu_H]^2 + \sigma[\mu_{HG}]^2}}, \qquad (2)$$

where $\sigma[\mu]$ represent the uncertainties.

Next, we convert the proper motion anomalies in the unit of mas yr^{-1} into the differential velocities in the unit of m s^{-1} as follows (Kervella et al. 2019):

$$\Delta v_{G[m\ s^{-1}]} = \frac{\Delta \mu_G [\text{mas yr}^{-1}]}{\varpi[\text{mas}]} \times 4740.47$$

$$\Delta v_{H[m\ s^{-1}]} = \frac{\Delta \mu_H [\text{mas yr}^{-1}]}{\varpi[\text{mas}]} \times 4740.47 \qquad (3)$$

where ϖ is the parallax in the unit of milliarcsecond. For a binary system, the differential velocity is approximately the projected tangential velocities of the primary's orbital motion on the sky plane (Kervella et al. 2019). Based on Kepler's law, the differential velocities are proportional to the companion masses (m_c) and inversely proportional to the square root of orbital distances (r): $\Delta v \propto \frac{m_c}{\sqrt{r}}$. Due to the observing window smearing effect (for details see Kervella et al. 2019), the proper motion anomalies method is most sensitive to companions with orbital periods longer than observing windows of Hipparcos and Gaia ($\delta_H = 1227$ days, Perryman et al. 1997, $\delta_{GDR3} = 1038$ days, Gaia Collaboration et al. 2022). On the other hand, the efficiency of the proper motion anomalies method drops for companions at orbital periods much longer than the 25 yr baseline between the two missions. For instance, the efficiency is reduced to $\sim$30% when the orbital period is 10 times the time baseline ($\sim$250 yr; Kervella et al. 2019).

Therefore, the sweet spot of proper motion anomalies is for companions at orbital periods from $\sim$3 yr up to $\sim$250 yr, corresponding to a few AU to dozens of AU in terms of the semimajor axis. Multiple studies have found a deficiency of planets in close binaries with separation below 100 au, supporting the theory of close companions disturbing and preventing planet formation (Kraus et al. 2016; Ziegler et al. 2020; Fontanive & Bardalez Gagliuffi 2021; Hirsch et al. 2021; Cadman et al. 2022). Hipparcos and Gaia astrometry thus offer an efficient way to search for planets in binaries that have separations of <100 au, with which we can study the effect of companions on planet formation and evolution.

3. Target Selection

3.1. Methodology

We constructed our target sample from host stars of transiting planet candidates, including TOIs/KOIs and K2 planet candidates. We used 4763 KOIs (2402 confirmed planets) from Kepler (Batalha et al. 2013; Burke et al. 2014; Mullally et al. 2015; Rowe et al. 2015; Coughlin et al. 2016; Thompson et al. 2018), 1547 K2 planet candidates (569 confirmed planets) from the K2 mission (Howell et al. 2014; Huber et al. 2016; Pope et al. 2016; Kostov et al. 2019; Zink et al. 2021), and 6682 TOIs (360 confirmed planets) from TESS (Guerrero et al. 2021). We downloaded the TOI/KOI/K2 lists from the NASA Exoplanet Archive[21]. Next, we used the Hipparcos and Gaia proper motion anomalies as an indicator to search for hidden companions to the planet or planet candidate hosts. Our procedure for selecting targets is as follows:

1. We crossmatched KOI/K2/TOI lists with HGCA using their R.A. ($\Delta \alpha < 10''$), decl. ($\Delta \delta < 10''$), and parallax ($\Delta \varpi / \varpi_{Gaia} < 20\%$).
2. We calculated the distance of targets with Gaia DR3 parallax and selected stars with distances smaller than 300 pc.
3. We calculated the S/N of Gaia's proper motion anomalies of every star from the last step. We selected those showing Gaia proper motion anomalies with $\geqslant 3\sigma$ significance (S/N$_G \geqslant 3$) into our target sample. Hereafter, we refer to our sample as HGCA high-S/N stars or stars with significant proper motion anomalies.
4. We also constructed a control sample of TOI stars with S/N$_G < 3$. Hereafter, we refer to the control sample as HGCA low-S/N stars or stars with marginal proper motion anomalies.

There are a total of 66 systems (58 TOIs, four KOIs, and four K2 planet candidates) in our target sample with high-S/N proper motion anomalies (see Table 1). We also identified 254 TOIs with low-S/N proper motion anomalies in the control sample and listed them in Appendix C and Table 5. The HGCA provides a parameter called χ^2, which represents the chi-squared value obtained from fitting a constant proper motion to the more precise pair of $\mu_{HG} - \mu_G$ and $\mu_H - \mu_{HG}$ proper motion measurements (Brandt 2021). This parameter is also helpful in evaluating the significance of proper motion anomalies. For instance, a χ^2 value of 11.8 corresponds to evidence of 3σ for proper motion anomalies. We compare the output samples

---

[21] https://exoplanetarchive.ipac.caltech.edu/

Table 1
TOI/KOI/K2 with Significant Proper Motion Anomalies

Name	HIP Number	P_{pl} days	Disposition in NASA Exoplanet Archive[a]	Disposition in This Work	Δv_G m s^{-1}	S/N$_G$	RUWE	Distance[b] pc	Comp. Sep. arcsec/ References
TOI-1684	20334	1.16	PC	PC	4176.05	226.52	1.58	87.11	⋯
TOI-510	33681	1.35	APC	PC	2700.32	116.11	2.43	92.84	5.5 (5)
TOI-394	15053	0.39	APC	EB	6995.08	94.97	3.18	141.7	3.22 (1)
TOI-6260	45961	2.39	PC	PC	6370.56	93.02	4.5	115.75	⋯
TOI-271	21952	2.48	APC	PC	8067.66	79.79	8.47	99.93	0.146 (2)
TOI-1124	98516	3.52	APC	EB	6904.05	53.18	11.77	80.17	⋯
TOI-896	28122	3.53	FA	FA	3091.52	45.59	1.4	155.53	0.062 (2)
TOI-5811	102295	6.25	PC	PC	2749.69	34.99	1.84	167.79	⋯
TOI-1418	83168	0.68	FA	SV	812.81	30.36	0.92	159.34	⋯
TOI-953	21000	2.97	FP	EB	6963.46	30.07	0.93	202.99	4.42 (1)

Notes.

[a] The flags come from the NASA Exoplanet Archive. CP: confirmed planet, PC: planet candidate, APC: ambiguous planet candidate, FP: false positive, FA: false alarm (Akeson et al. 2013).

[b] Distances are from Gaia DR3 (Gaia Collaboration et al. 2022).

[c] Single transit PC, no orbital period.

[d] Multiple planet systems.

References. Companion separation from published papers or TFOP. The references are (1). Ziegler et al. (2020, 2021); (2). Lester et al. (2021); (3). TFOP, observation using Palomar/PHARO (PI: D. Ciardi); (4). Rodriguez et al. (2015), Winters et al. (2019); (5). Washington Double Star (WDS) catalog (Mason et al. (2001); (6). GP: the proper motion anomalies of TOI-144, TOI-1144, and TOI-1339 are from giant planets (Damasso et al. 2020; De Rosa et al. 2020; Xuan & Wyatt 2020; Lubin et al. 2022); (7). Dupuy et al. (2016), Zhang et al. (2023). (8). Zhou et al. (2022).

(This table is available in its entirety in machine-readable form.)

using the criteria of $\chi^2 \geqslant 11.8$ and S/N$_G \geqslant 3$. The two criteria are nearly equivalent, resulting in comparable samples.

3.2. Target Sample

Figure 2 presents a color-absolute magnitude diagram of 66 selected targets (58 TOIs, four KOIs, and four K2 planet candidates), color coded by the significance of Hipparcos-Gaia proper motion anomalies. We calculated the absolute magnitude using $M_G = m_G + 5 \log d + 5$, where m_G and d are Gaia G-band apparent magnitude and distance. Most of our targets are main-sequence stars with $0.5 < G_{Bp} - G_{Rp} < 1.5$ and $0 < M_G < 7$. We highlight stars with multiple transiting planets in Table 1, including TOI-402 (Dumusque et al. 2019; Gandolfi et al. 2019), TOI-455 (LTT 1445 Winters et al. 2019, 2022), TOI-144 (π Men Jones et al. 2002; Gandolfi et al. 2018; Hatzes et al. 2022), TOI-201 (Hobson et al. 2021), TOI-1339 (HD 191939, Badenas-Agusti et al. 2020; Lubin et al. 2022; Orell-Miquel et al. 2023), TOI-1730 (Simpson & Cloutier 2022), and KOI 03158 (Kepler-444, Campante et al. 2015).

Some targets in our sample have been investigated before. The triple system Kepler-444 consists of a primary star with five transiting Mars-sized and Mars-mass planets. Dupuy et al. (2016) and Mills & Fabrycky (2017) characterized the Kepler-444 BC companion pair as orbiting the primary A in a highly eccentric orbit ($e \sim 0.864$, $a \sim 5$ au) using RVs and relative astrometry from imaging. Recently, Zhang et al. (2023) improved the constraints on the orbit of the Kepler-444 BC pair ($e \sim 0.55$, $a \sim 36$ au, $i \sim 85°.4$) using a longer time baseline of RVs and the proper motion anomalies data from the Hipparcos and Gaia missions. Both studies suggest that Kepler-444 BC may have truncated the protoplanetary disk of the primary, resulting in the small sizes of the system's five planets. Zhou et al. (2022) characterize the 3D orbit of an M dwarf companion to TOI-4399 (HIP 94235), which hosts a mini-Neptune with an orbital period of 7.1 days. Their results show that the companion has a semimajor axis of $\sim$60 au
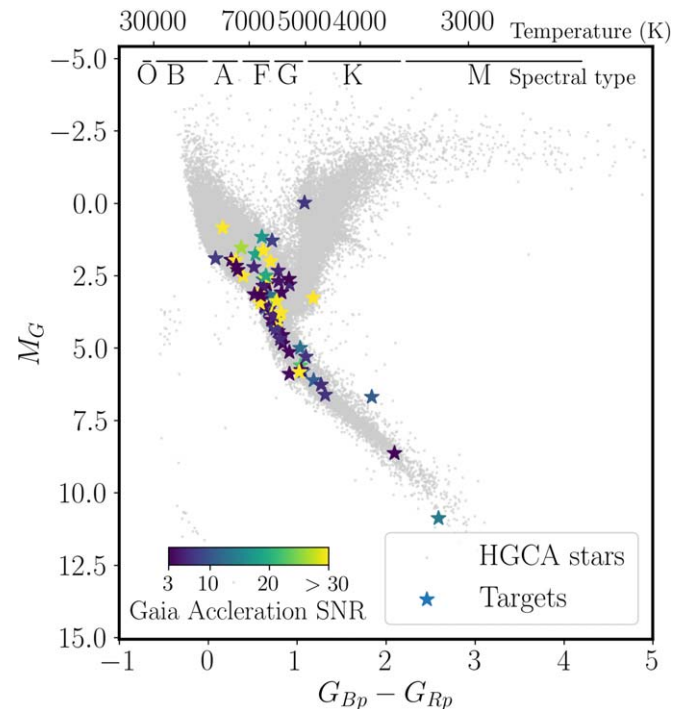

Figure 2. Gaia color-absolute magnitude diagram for our targets (star signs) and stars in HGCA within 300 pc (gray dots). TOI/KOI/K2 planet candidate hosts with significant proper motion anomalies are color coded by the S/N of their proper motion anomalies at the Gaia epoch (S/N$_G$).

and an inclination of $\sim$67°.8, indicating a modest misalignment between the companions and the transiting planet. Furthermore, previous studies have identified that the Hipparcos and Gaia proper motion anomalies of TOI-144 (π Men, Damasso et al. 2020; De Rosa et al. 2020; Xuan & Wyatt 2020), TOI-1144 (HAPT-11, Xuan & Wyatt 2020), and TOI-1339 (HD 191939, Lubin et al. 2022) are from giant planets at a few AU. By combining the
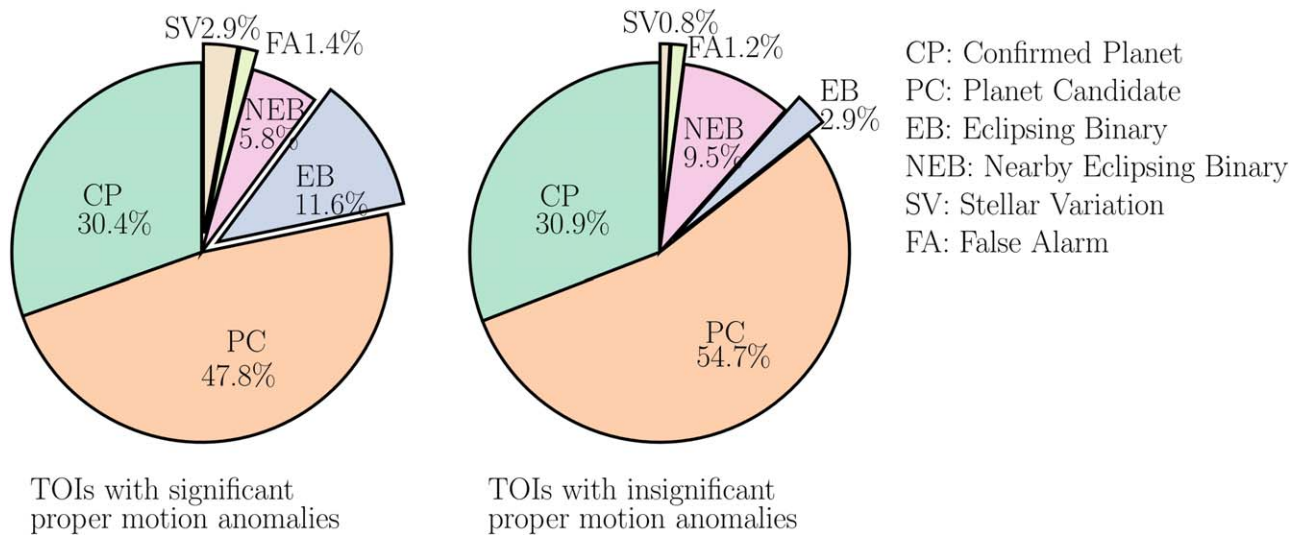
Figure 3. Right panel: the fraction of CPs, planet candidates, and several FPs of TOIs in our high-S/N sample. Left panel: the fraction of the same categories but for low-S/N TOIs. The two samples are both limited to 300 pc. We only present TOIs in this figure because the majority of KOI/K2 targets in our sample are EBs.

proper motion anomalies and RVs, these studies obtained a constraint on the semimajor axis, orbital inclination, and mass of the giant planets.

Among the sample of 66 targets with high proper motion anomalies, 33 systems have confirmed companions from previous surveys using AO/speckle imaging, mostly at separations from $0.''1$–$2''$. In Table 1, we list the companion separations from published papers (Mason et al. 2001; Kraus et al. 2016; Winters et al. 2019; Ziegler et al. 2020; Howell et al. 2021; Lester et al. 2021; Ziegler et al. 2021) and the TESS Follow-up Observing Program (TFOP). Additional AO imaging using Keck/NIRC2 and Subaru/SCExAO will be presented in a follow-up paper.

4. Statistical Analysis of TOIs

4.1. Planet Candidates versus False Positives

We first analyzed the fraction of false positives of the transiting detections in the sample. Table 1 lists the NASA Exoplanet Archive dispositions that classify TOIs/KOIs/K2 candidates, including confirmed/known planets (CPs/KPs), planet candidates (PCs), ambiguous planet candidates (APCs), false positives (FPs), and false alarms (FAs). We also present different reasons for the FP/FA dispositions in Table 1. An FP or FA flag is assigned in several situations. The first scenario is eclipsing binaries (EBs), in which the secondary stars graze the edge of primaries, and the reduction in brightness is indistinguishable from transits of smaller planets. The second scenario is the contamination by a nearby eclipsing binary (NEB) as multiple stars are unresolved due to the large pixel scale of Kepler and TESS ($4''$ for Kepler and $21''$ for TESS). In this case, the bright primary star dilutes the light of a nearby, dimmer, EB pair to the point at which the eclipses seem as shallow as a planetary transit. In addition, stellar variation (SV) and spacecraft systematic errors can also mimic the dips in light curves similar to those from transiting planets.

To break down the FP into the EB/NEB/SV flag, we refer to the TESS Follow-Up Observing Program Sub-Groups 1 and 2 (TFOPs SG1 and SG2) disposition and notes as a guide for TOIs. TFOP SG1 performs seeing-limited imaging of the TOIs using ground-based telescopes with higher spatial resolution to

check whether the transits occur on target. They detected four TOIs (TOI-2118, TOI-1665, TOI-909, TOI-1946) in our sample as NEB. In addition, TFOP SG2 identified eight EBs based on an odd–even transit difference (TOI-394, TOI-1124, TOI-575,) or RVs from TRES+FIES (TOI-953, TOI-1837, TOI-2017, TOI-2666, TOI-222). In our sample, the majority of KOIs and K2 transiting signals are from EBs based on the results from the Kepler/K2 EB catalogs (Slawson et al. 2011; Armstrong et al. 2015; Rizzuto et al. 2017; Kruse et al. 2019). We present the details of each FP in our sample in Appendix A.

The left panel in Figure 3 presents the fraction of CPs, PCs, EBs, NEBs, and other FPs in TOIs with significant proper motion anomalies (58 TOIs). We have chosen to only present the results of TOIs for a homogeneous comparison because follow-up observations for candidates of TOI, KOI, and K2 are conducted through various projects, and the majority of KOIs and K2 targets in our sample are EBs. For comparison, we show a control sample from TOIs with $S/N_G < 3$ and distances smaller than 300 pc (254 TOIs). We also break down the FPs in the HGCA low-S/N sample into the same categories as our targets based on the TFOP SG1 disposition. The HGCA high-S/N TOIs contain a higher fraction of FPs (up to 21.8% compared to the 14.4% of HGCA low-S/N TOIs). The difference is mainly from the excess of EBs among the HGCA high-S/N TOIs, taking up ~11.6% of the sample. The EB FPs result from the contamination of triple systems with close-in EBs. Due to the dilution of light curves by multiple sources in the same pixel, the transit depth appears comparable to planetary transits around single stars. Our finding agrees with previous studies. Ziegler et al. (2020) present that hot Jupiters are more common in binaries with wide companions compared to field stars. But Ziegler et al. (2021) argue that these findings can be attributed to FP contamination arising from tertiary companions to closely orbiting EBs. In contrast, other FPs, including NEBs, stellar variability, and spacecraft FAs, account for a similar share in the two samples.

4.2. Orbital Period of TOIs with Significant Proper Motion Anomalies

In this section, we compare the orbital periods of planets around TOIs with significant Hipparcos-Gaia astrometric
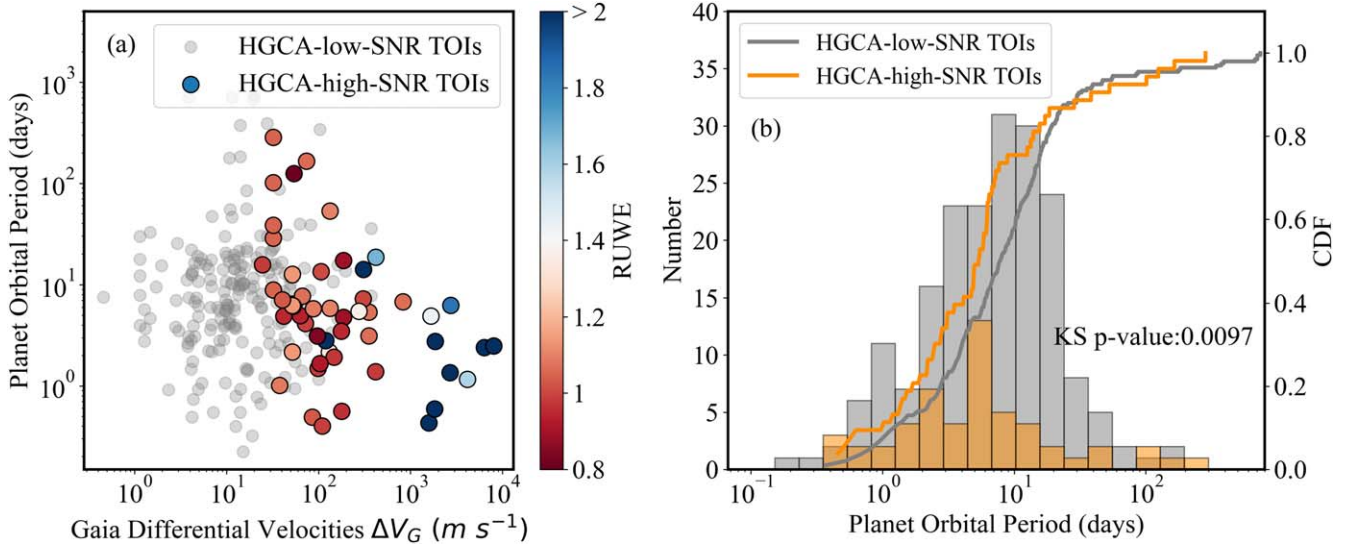
Figure 4. Panel (a): planet orbital period vs. differential velocities at Gaia epoch of TOIs with significant proper motion anomalies (color coded by their Gaia DR3 RUWE) and TOIs with marginal proper motion anomalies (gray). We exclude TOIs with FP/FA dispositions. High-S/N TOIs with RUWE $\geqslant 1.4$ are in red, whereas those with RUWE < 1.4 are in blue. Panel (b): marginalized distribution of planet orbital periods of high (orange) and low (gray) S/N TOIs overlapped with the cumulative distribution function. We exclude TOIs with FP/FA dispositions.

acceleration and those with marginal astrometric acceleration. Figure 4(a) presents the planet orbital periods and the Gaia differential velocities of TOIs with high-S/N and low-S/N proper motion anomalies, respectively. The Gaia differential velocities are defined in Section 2 (see Equation (3)) We exclude systems with FP and FA dispositions. We do not include the eight KOIs and K2 targets because seven of them are FPs. We colored HGCA high-S/N TOIs by their Gaia DR3 RUWE. An RUWE value greater than 1.4 usually indicates that the source is non-single and the two components are too close to be fully resolved by Gaia (Lindegren et al. 2018).

The HGCA high-S/N TOIs with high RUWE mostly have differential velocities beyond 1000 m s^{-1}, including TOI-271, TOI-680, TOI-930, TOI-1719, and TOI-1131. The high differential velocities are consistent with these TOIs having close stellar companions with separations below 1″ (see Table 1[22]). In comparison, HCGA high-S/N TOIs with low RUWE have differential velocities from dozens to a few hundred m s^{-1}. In some systems, the velocities in the middle range are from stellar companions at relatively wider separation. For instance, TOI-402, TOI-4175, TOI-635, and TOI-128 are all in this regime and have companions with separations $>1″$. In other cases, low-mass companions, such as brown dwarf companions and giant planets, cause the primaries to orbit around the barycenter at velocities from dozens to a few hundred m s^{-1}. Their low RUWE indicates that the single-star model is still a good fit because the substellar companions are much fainter than primaries. In our sample, the Hipparcos-Gaia proper motion anomalies reveal the existence of giant planets at a few AU in TOI-144 (π Men), TOI-1144 (HAPT-11), and TOI-1339 systems.

Figure 4(a) shows a tentative inverse correlation between the orbital period of transiting planets and the Gaia differential velocities of their host stars. The planet periods of TOIs with differential velocities >1000 m s^{-1} are all shorter than 10 days.

Figure 4(b) displays the distributions of planet orbital periods of HCGA high-S/N and HCGA low-S/N TOIs. We include 53 HCGA high-S/N TOIs and 200 HCGA low-S/N TOIs. We can see that orbital periods of transiting planets in HCGA high-S/N TOIs are generally shorter than in HCGA low-S/N TOIs. A Kolmogorov–Smirnov test shows that the difference between two samples' planet orbital period distributions is statistically significant (p-value $= 9.7 \times 10^{-3}$).

To explore whether the trend found in Figure 4 holds true for a larger sample, we compare the orbital periods of planets in binary and single TOIs/KOIs from Kraus et al. (2016), Ziegler et al. (2020), Howell et al. (2021), Lester et al. (2021), and Ziegler et al. (2021). Figure 5(a) presents the stellar companion separations and planet orbital periods of these TOIs and KOIs. In Figure 5(b), We include 265 and 56 CPs in binary and single TOIs from Ziegler et al. (2020), Howell et al. (2021), Lester et al. (2021), and Ziegler et al. (2021). In Figure 5(c), we include 138 and 296 CPs in binary and single KOIs from Kraus et al. (2016). To rule out the influence of EBs that usually have short periods, we only select CPs or KPs from their sample. We also removed duplicate TOIs resulting from the overlap between different surveys. We did not apply a distance cutoff to their sample, as such an approach would have resulted in a further decrease in the size of the sample. But most of their targets are within 400 pc, with a small fraction extending beyond 800 pc (see Figure 1 in Kraus et al. 2016; Ziegler et al. 2021). We find that TOIs in binaries have orbital periods statistically shorter than those in single systems (p-value $= 0.0016$). However, we do not see a significant difference between confirmed Kepler planets in binaries and singles (p-value $= 0.82$).

A few possibilities can explain the different results in the TOI and KOI samples. First, the difference in sensitivity between the two missions may explain the observed disparity, as TESS detected more short-period planets within 10 days but fewer at longer periods than Kepler. However, this explanation alone cannot account for the shorter orbital periods of planets in binary TOIs, since TESS searches for planets without considering the binarity of the targets. The second possibility

---

[22] Except for TOI-510, which has a companion at 5″5 reported from the WDS catalog. The Hipparcos-Gaia acceleration indicates there might be another unresolved companion at a closer separation.
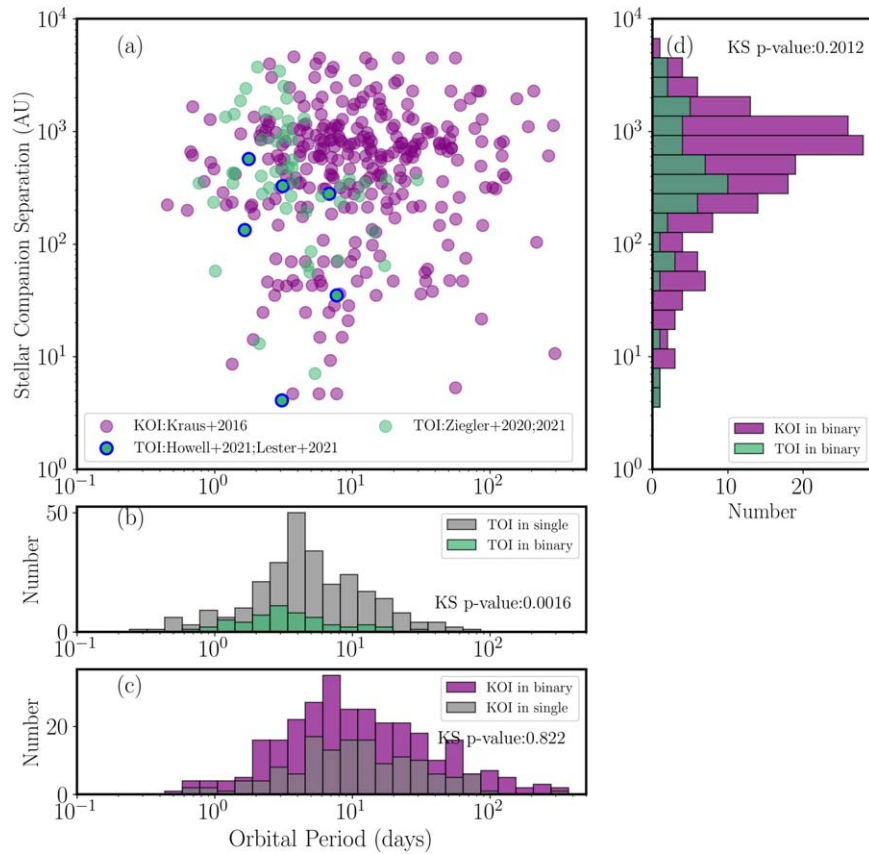
Figure 5. Panel (a): planet orbital period versus stellar companion separations of TOIs (green, Ziegler et al. 2020; Howell et al. 2021; Lester et al. 2021; Ziegler et al. 2021) and KOIs (purple, Kraus et al. 2016) in binary systems. We only include CPs or KPs. Panel (b): marginalized distribution of planet orbital periods of TOIs in binaries (green) and singles (gray). Panel (c): same as panel (b) but for KOIs in binary (purple) and single (gray) systems. Panel (d): marginalized distribution of stellar companion separations of TOIs (green) and KOIs (purple) in binaries.

is that stellar companions in the KOI sample have relatively larger separations as they are generally more distant and fainter than TOIs. Therefore, companions in the KOI sample are less influential in shaping the planets' orbital periods. Ziegler et al. (2020, 2021) and Kraus et al. (2016) both present stellar companions to KOIs/TOIs at separations from a few AU to a few thousand AU. However, Figure 5(d) illustrates that the distributions of stellar companion separations in the TOI and KOI samples do not exhibit a significant difference (p-value = 0.20). Third, the difference between binary and single TOIs might potentially be attributed to the relatively small size of TOIs in binary systems. Therefore, a larger sample of TOIs in binaries is required to reach a more decisive conclusion. Finally, the disparity in planet periods observed between the TOI and KOI samples may be due to the fact that Kepler has higher precision and is thus more sensitive to smaller planets than TESS. Consequently, the two missions may be observing different populations of planets. To test the hypothesis, we need to revise the radii of planets orbiting TOIs/KOIs in binary systems by accounting for the flux dilution.

In short, the reason why the TESS bias affects binary and single systems differently is not yet understood, and a larger sample of TOIs is needed to draw a more definitive conclusion. If the TOIs in binaries do have shorter orbital periods (<10 days), they might form in truncated disks by the companions. Besides, planets' survival probability is likely higher at close-in orbits because the host stars provide more shield to resist the gravitational disturbance from the companions.

4.3. Differential Velocity Distribution of TOIs versus Field Stars

As detailed in Section 2, the differential velocities can be approximately seen as the projected orbital velocities of the primary stars around the system barycenter, which increases with the companion masses and decreases with orbital distances. In this section, we compare the Gaia differential velocities of HCGA high-S/N TOIs with field stars, which consists of all stars exhibiting significant proper motion anomalies from HGCA within 300 pc. Figure 6 presents the results. The differential velocities of field stars exhibit a peak around 3000 m s^{-1} and a broader bump centered at ∼200 m s^{-1} to the left. The velocity magnitude at the peak is consistent with differential velocities caused by stellar companions with orbital periods from a few years to a few hundred years (sensitive range for Hipparcos-Gaia proper motion anomalies method). For example, a solar mass star would have a differential velocity of around 4400 m s^{-1} with a 0.5 $M_{\odot}$ companion at an orbital period of approximately 25 yr, assuming a face-on orbit. As the orbital periods increase or companion masses decrease, the stellar companions' velocities produce a tail at lower velocities. For example, a 0.01 $M_{\odot}$ companion would cause a velocity of around 100 m s^{-1} for a solar mass star over a 25 yr period.

Compared to field stars, the distribution of HCGA high-S/N TOIs displays a higher peak at velocities around 100 m s^{-1} with a shortfall at high differential velocities. These distributions suggest that transiting planets are more likely to form in
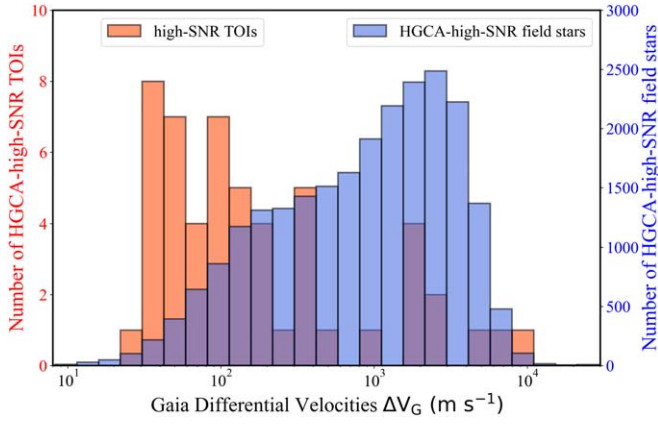
Figure 6. Gaia differential velocity distribution of TOIs with significant proper motion anomalies (red) compared to field stars (blue). The field star sample consists of all stars with significant proper motion anomalies from HGCA within 300 pc. The differential velocities are in log scale. We exclude TOIs with FP/FA disposition.

binaries when the companions have lower masses or are at wider separations. Our results are compatible with the previous studies that planets are less common in close binary systems compared to single systems or wide binaries (Wang et al. 2015; Kraus et al. 2016; Ziegler et al. 2020; Hirsch et al. 2021; Moe & Kratter 2021; Ziegler et al. 2021). In a recent study, Moe & Kratter (2021) found that the occurrence rate of planets in binaries with $a < 10$ au is roughly 15% of that in single systems, while wide binaries with $a > 200$ au have planet occurrence rates similar to those of single stars. Recent ALMA high-resolution surveys also find that disks in multiple systems are smaller, fainter, and less long-lived than those in singles (Cox et al. 2017; Akeson et al. 2019; Manara et al. 2019; Zurlo et al. 2020; Zagaria et al. 2023). These findings support the theory that close companions tidally truncate the circumstellar disks and reduce the reservoir of material available to assemble planetary embryos (Paczynski 1977; Rudak & Paczynski 1981; Pichardo et al. 2005; Jang-Condell et al. 2015; Zagaria et al. 2023).

5. Orbit Characterization of the Benchmark System: LTT 1445 ABC

In this section, we present the results of the proof-of-concept system LTT 1445 ABC, for which we characterize the three-dimensional orbits of the companion pair BC around A with RVs, Hipparcos-Gaia astrometric acceleration, and relative astrometry from AO imaging.

5.1. Background

LTT 1445 ABC (TOI-455) is the closest M dwarf triple known to harbor multiple planets at a distance of 6.86 pc (Rossiter 1955; Luyten 1957, 1980; Winters et al. 2019, 2022). The hierarchical system consists of a primary LTT 1445 A ($0.268 R_\odot$, $0.257 M_\odot$) orbited by a M dwarf pair BC at a separation of $\sim 7''$ (Dieterich et al. 2012; Rodriguez et al. 2015). LTT 1445 A has two transiting super-Earths and one non-transiting planet: LTT 1445 Ab ($P_b = 5.36$ days, $r_b = 1.3 R_\oplus$, $m_b = 2.87 \pm 0.25 M_\oplus$), LTT 1445 Ac ($P_c = 3.12$ days, $r_c < 1.15 R_\oplus$, $m_c = 1.54 \pm 0.2 M_\oplus$), LTT 1445 Ad ($P_b = 24.3$ days, $m_d = 2.72 \pm 0.25 M_\oplus$) (Winters et al. 2019; Lavie et al. 2023; Winters et al. 2022). The BC subsystem is a visual binary pair with a separation of $\sim 1''$. Using archival

Table 2
LTT 1445 A RVs

Time (BJD-2450000)	RV (m s^{-1})	σ_{RV} (m s^{-1})	Inst.
9482.1	1.69	1.37	HIRES
9587.81	−1.54	1.37	HIRES
9824.13	2.33	1.29	HIRES
9832.03	3.5	1.46	HIRES
9947.73	0.45	1.2	HIRES

Note. Times are in BJD-2450000.0. The RV uncertainties do not include RV jitter. We present five unpublished HIRES RVs in this table. All RV data utilized in the orbit fitting, including those sourced from the literature, are available in a machine-readable format.

(This table is available in its entirety in machine-readable form.)

astrometry from Fourth Interferometric Catalog and Differential Speckle Survey Instrument, Winters et al. (2019) found that LTT 1445 C orbits around B in an eccentric and edge-on orbit with a period of ~ 36 yr ($e_{C,B} = 0.5 \pm 0.11$, $i_{C,B} = 89^\circ.64 \pm 0^\circ.13$, $a_{C,B} = 8.1 \pm 0.5$ au, $\Omega_C = 137^\circ.63 \pm 0^\circ.19$). However, it is unclear how the companion pair orbit around the primary. Therefore, we utilized the Hipparcos-Gaia proper motion anomalies, combined with primary RVs and relative astrometry to characterize the orbit of the LTT 1445 BC pair around the primary A. Furthermore, we constrain the mutual inclination between the orbital plane of C around B and that of the subsystems around the primary. LTT 1445 A is targeted by the James Webb Space Telescope Cycle 1 GO Program 2708 (PI: Z. Berta Thompson) to investigate the presence of an atmosphere on the planet b. Our characterization of the companion pair's orbit provides context for the dynamical stability of the system.

5.2. Orbit Fitting

We use nine archival RVs of LTT 1445 A taken with HARPS between 2004 and 2013 from Trifonov et al. (2020) and 136 published RVs from 2019–2021 taken with five high-precision spectrographs including the W. M. Keck Observatory echelle spectrograph HIRES, ESPRESSO, HARPS, MAROON-X, and Planet Finder Spectrograph (PFS) from Winters et al. (Winters 2022). We also include five RVs we newly collected between 2021 September and 2023 January using HIRES (see Table 2). The proper motion anomalies of LTT 1445 A at Hipparcos and Gaia epoch are from HGCA. Finally, we adopt two published relative astrometric measurements taken in 2003 and 2010 from Dieterich et al. (2012) and Rodriguez et al. (2015; see Table 3). We consider the BC pair as one object and use the relative astrometry of the mass center of the BC subsystem to primary A.

We use open source package orvara (Brandt et al. 2021), which performs a parallel-tempering Markov Chain Monte Carlo (MCMC) fitting. In total, our analysis uses 15 free parameters. Two of them are the masses of the host star (M_A) and the combined mass of the companion pair (M_{BC}). Six orbital parameters define the orbit of the companion pair, including semimajor axis (a), inclination (i), longitude of the ascending node (Ω), mean longitude at a reference epoch (2455197.5 JD) (λ_{ref}), and the eccentricity (e) and the argument of periastron (ω) in the form of $e \sin \omega$ and $e \cos \omega$. We also included six parameters to fit the zero-point for RV data from different instruments. As there was a fiber exchange

Table 3
Relative Astrometry Used in the Orbit Characterization for LTT 1445 BC around A

Date		θ (°)	ρ ('')	Instrument	Reference
2003.4620	A–B	315.0	7.706	HST/NICMOS	(1)
2003.4620	B–C	138.1	1.344	HST/NICMOS	(1)
2003.4620	A–BC[a]	314.74	7.13	HST/NICMOS	(3)
2010.594	A–B	313.79[b]	7.20	Lick/IRCAL	(2)
2010.594	B–C	138.41	0.41	Lick/IRCAL	(2)
2010.594	A–BC	314.91	7.02	Lick/IRCAL	(3)

References. (1) Dieterich et al. (2012); (2) Rodriguez et al. (2015); (3) Derived in this work.
[a] Relative astrometry of the mass center of BC from A.
[b] The quadrant is ambiguous; the position angle here has been changed by 180° relative to the original result.

for HARPS in 2015, we use different RV zero-points for HARPS RVs taken before and after 2015. The last parameter is the intrinsic jitter of RV data. We ignore the transiting planets because their RVs amplitudes are expected to be smaller than the stellar jitter. The proper motion anomalies from inner planets are also nearly zero because signals cancel out when the orbital periods are much shorter than the observing window duration of Hipparcos and Gaia. We use the primary mass and companion masses from Winters et al. (2019) as priors in our fitting and bound the jitter between 0 and 10 m s^{-1}. The likelihood is calculated by comparing the measured separations, position angles, absolute astrometry, and radial velocities to those of a synthetic orbit and assuming Gaussian errors (Brandt et al. 2021).

We use 100 walkers to sample our model and the chains converge after 2.5×10^5 steps. We discarded the first 30% as burn-in portion. The joint MCMC posterior distribution of the parameters are shown in Figure B.1. Figure 7 shows the best-fit orbit (black lines) from our MCMC chains, including fitted astrometric orbit, RVs, and Hipparcos-Gaia proper motions (the observed and fitted absolute astrometry from AO imaging are shown in Figure B2). The reduced χ^2 of RVs indicates a good fit and accurate measurement errors, with values of 0.97. We obtain a dynamic mass of $M_A = 0.251^{+0.010}_{-0.010}\ M_\odot$ for primary A and a mass of $M_{BC} = 0.39^{0.009}_{-0.009}\ M_\odot$ for the BC subsystem, which agree with the published values from Winters et al. (2022) within 1σ. Our best-fit model shows that the subsystem BC orbits around primary A in an eccentric and edge-on orbit ($a_{BC,A} = 58^{-20}_{+16}$ au, $e_{BC,A} = 0.375^{+0.037}_{-0.064}$, $i_{BC,A} = 88°.5^{+1.3}_{-1.4}$, $\Omega_{BC,A} = 135°.15 \pm 0°.28$, see Table 4 for other parameters). We compute the mutual inclination ΔI between the orbital plane of BC around A and that of C around B with their inclination ($i_{C,B}$, $i_{BC,A}$) and longitude of ascending node ($\Omega_{C,B}$, $\Omega_{BC,A}$):

$$\cos \Delta i = \cos i_{C,B} \cos i_{BC,A} + \sin i_{C,B} \sin i_{BC,A} \cos(\Omega_{C,B} - \Omega_{BC,A}). \quad (4)$$

We obtained the mutual inclination $\Delta i = 2°.88 \pm 0°.63$. Therefore, LTT 1445 ABC is a flat system where the subsystem BC orbits around A in nearly the same plane as their orbit around each other. Because the LTT 1445 A is a slow rotator ($P_{tot} \sim 84$ days, Winters et al. 2019), we are not able to measure the spin–orbit angle of two transiting planets b and c relative to the primary through the Rossiter–MacLauglin effect. However, the probability of observing the two transiting

planets and companion pair BC all have edge-on orbits is notably low, if we assume their orbits are independent. Specifically, if the $\cos(i)$ values of planets b, c, and companion pair BC are drawn randomly from a uniform distribution between 0 and 1, the probability of observing all these bodies to have inclinations within the range of 87°–90° is only 0.014%. Therefore, it is highly likely that the transiting planet orbits are coplanar with the orbit of the BC companions. Meanwhile, the alignment of the non-transiting planet LTT 1445 Ad with the inner planets is subject to significant uncertainty. Located at a distance of 0.09 au, the angle range for a transiting configuration is only 1°.6. A plausible scenario is that LTT 1445 Ad is aligned with the inner planets but is located outside the transiting configuration. A detailed dynamical study might yield interesting constraints on the possible orbits of planet d, but is beyond the scope of this paper.

5.3. Implication for Planet Formation

One piece that needs to be added to understand the effect of companions on planet formation is the inclination of the companion orbits. Inclination plays a vital role in the dynamic interaction between the companions and inner planets or the protoplanetary disks. For example, the Kozai–Lidov effect (Kozai 1962; Lidov 1962) occurs when the mutual inclination between two objects is greater than $\sim 40°$, causing the inner objects to be unstable. Previous studies have also found that inclined outer companions may cause the orbit of inner planets to be misaligned relative to their host stars (Huber et al. 2013; Zhang et al. 2021). Fortunately, the combination of Hipparcos and Gaia astrometry and RVs allows us to characterize the three-dimensional orbits of the companions. In this work, we present the results of triple system LTT 1445, in which LTT 1445 BC orbits around the primary A with a semimajor axis of ~ 58 au. The LTT 1445 system bears a remarkable resemblance to the Kepler-444 triple system, where Kepler-444 BC orbits around A in an edge-on orbit and is likely to be aligned with the orbit of five transiting planets around the primary A (Dupuy et al. 2016; Zhang et al. 2023). LTT 1445 and Kepler-444 both agree with the statistical results reported by Dupuy et al. (2022), which conclude that low mutual inclinations between planets and companions are required to explain the observed orbital arcs in 45 binary systems containing Kepler planet candidates. One may ponder whether the coplanarity of the systems relates to the planet's formation in a dynamically hostile environment.

Zanazzi & Lai (2018) investigated the evolution of disk inclinations in binary systems and found that effective realignment between the circumstellar disks around the primary star and companions tends to occur when the companions are closer than 200 au. Considering that LTT 1445 BC has a semimajor axis of ~ 58 au, it is plausible that the companions were initially misaligned with the primary disk but later underwent realignment during their evolution. Another close binary HIP 94235 ($a \sim 50$ au) is consistent with the possibility that the primary hosts a transiting mini-Neptune. The companion HIP94235B exhibits an inclination of around 68° (Zhou et al. 2022), which suggests a minimum misalignment of 22° between the companions and the transiting planet. Given that HIP 94235 is part of a young comoving group (~ 120 Myr, Zhou et al. 2022), it is possible that the realignment between the companion and the disk is still ongoing. Alternatively, it is
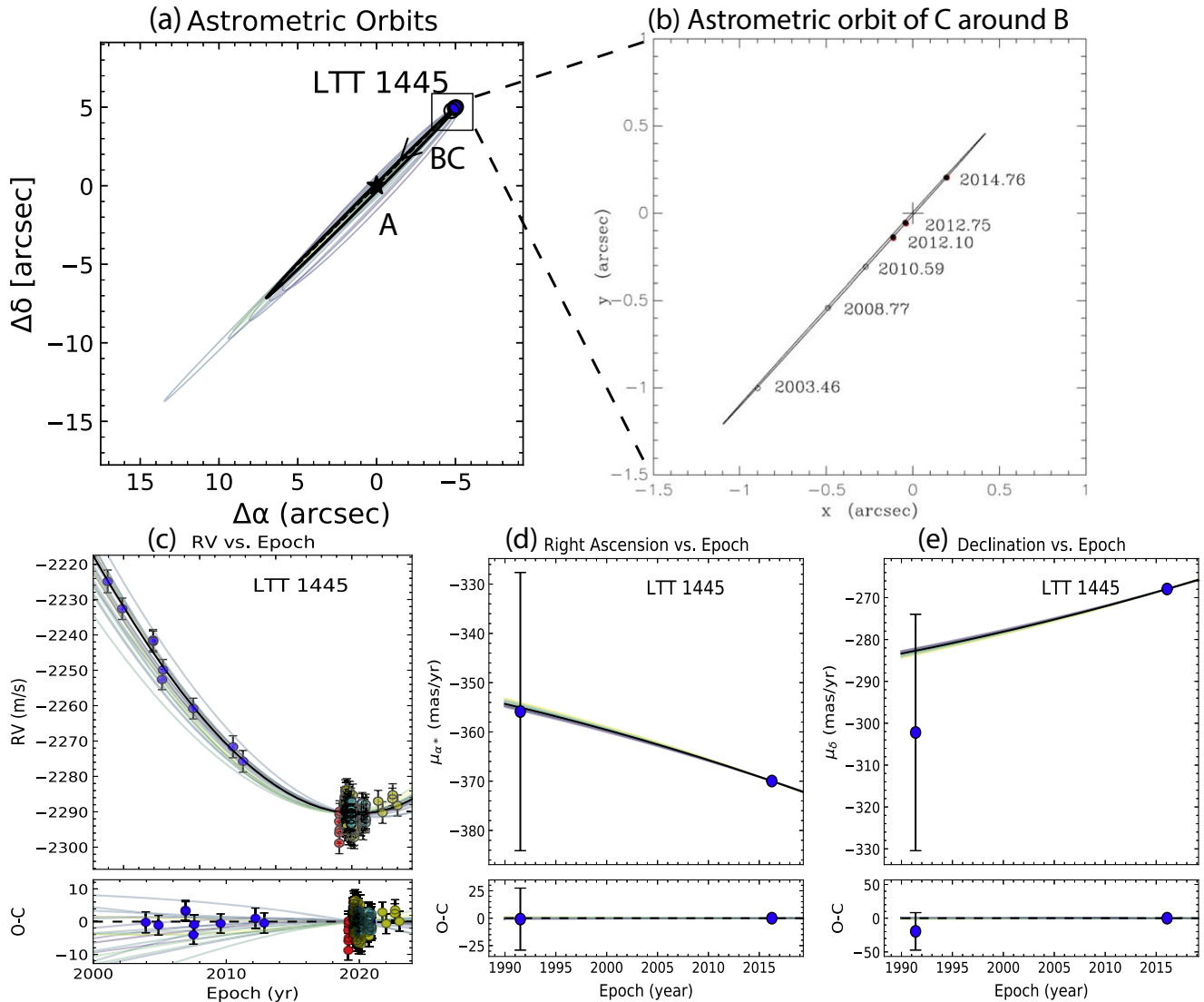
Figure 7. Orbit characterization of the LTT 1445 BC mass center around A using RVs, relative astrometry, and absolute astrometry from Hipparcos and Gaia. (a): relative astrometry orbits of LTT 1445 BC pair around A. The blue-filled circles are two observed relative astrometry used in our analysis. (c): Observed and fitted RVs of LTT 1445 from HARPS, HIRES, ESPRESSO, MAROON-X, and PFS. (d), (e): observed and fitted Hipparcos and Gaia proper motion of LTT 1445 A in R.A. and decl. In all of the above panels, the thicker black lines represent the best-fit orbit in the MCMC chain while the other 50 lines represent random draws from the chain; (b): relative astrometry orbits of LTT 1445 C around B from Winters et al. (2019).

also possible that the LTT 1445 BC was initially aligned with the primary disk from the onset. In this case, the fully conplanar configuration and close separation of LTT 1445 triples are consistent with the disk fragmentation scenario that gravitational instability in a shearing disk might produce multiple stars (Adams et al. 1989; Moe & Kratter 2018; Offner et al. 2023). In either possibility, although the companions likely truncated the primary's circumstellar disk, there was still enough disk material remaining to form multiple planets. In short, constraining the mutual inclination between planets and stellar companions in more systems is needed to understand the mechanisms behind planet formation in close binary systems.

6. Conclusions

We have presented a study of transiting planets with systems that show significant Gaia-Hipparcos accelerations. Our conclusions are as follows:

1. We presented a catalog of 66 transiting planet hosts (58 TOIs, four KOIs, and four K2 planet candidates) within a 300 pc volume limit with significant Hipparcos and Gaia proper motion anomalies through crossmatching the TOI/KOI/K2 catalogs with HGCA. The parameters of these targets are presented in Table 1. Among these targets, 33 have directly imaged stellar companions, either from published papers or the ExFOP website.

2. For transiting PCs identified by TESS, we evaluated the reliability of the transits based on the radial velocities obtained with Keck/HIRES and the TFOP. We found that TOIs with high proper motion anomalies have nearly four times more EB classifications than TOIs with insignificant proper motion anomalies. The excess of EBs in HCGA high-S/N TOIs might be from the contamination of triple systems.

3. We translated the proper motion anomalies into differential velocities between the epochs of Hipparcos and Gaia, expressed in m s^{-1}. We observe a tentative inverse

Table 4
MCMC Orbital Posteriors for LTT 1445

Parameter	Median $\pm 1\sigma$	Best-fit Value
Stellar parameters		
Host star mass M_A ($M_\odot$)	0.25 ± 0.01	0.25
Companion pair mass M_{BC} ($M_\odot$)	0.39 ± 0.09	0.39
Orbital parameters		
Semimajor axis a (AU)	58^{+16}_{-10}	63.45
Orbital period P (yr)	549^{+243}_{-136}	629.54
Inclination i (deg)	$88.5^{+1.3}_{-1.3}$	88.82
$\sqrt{e}\sin\omega$	$-0.568^{+0.036}_{-0.025}$	-0.24
$\sqrt{e}\cos\omega$	$-0.14^{+0.28}_{-0.24}$	-0.58
Eccentricity e	$0.375^{+0.084}_{-0.037}$	0.4
Mean longitude at $t_{\rm ref} = 2455197.5$ JD, $\lambda_{\rm ref}$ (deg)	210.3 ± -2.1	211.19
Longitude of the ascending node Ω (deg)	135.15 ± 0.28	135.10
Parallax (mas)	$145.6923^{+0.0040}_{-0.0040}$	145.69
Argument of periastron ω (deg)	256^{+28}_{-21}	247.52
Time of periastron $T_0 = t_{\rm ref} - P\frac{\lambda - \omega}{360}$ (JD)	2480796^{+5304}_{-5663}	2478401.65
Other parameters		
RV jitter σ (m s^{-1})	$2.74^{+0.21}_{-0.18}$	2.73
HARPS pre-2015 RV zero-point (m s^{-1})	3225.67^{+166}_{-177}	3162.27
HARPS post-2015 RV zero-point (m s^{-1})	-2188.44^{+166}_{-176}	-2250.74
EXPRESSO RV zero-point (m s^{-1})	3232.41^{+166}_{-177}	3169.01
MAROON-X RV zero-point (m s^{-1})	-2226.99^{+166}_{-177}	-2290.44
HIRES RV zero-point (m s^{-1})	-2225.24^{+166}_{-177}	-2288.68
PSF RV zero-point (m s^{-1})	-2226.55^{+166}_{-177}	-2289.98

Note. The χ^2 of relative astrometry is 0.09 for separations and 0.06 for PAs, with two measurements for each. The χ^2 of the Hipparcos and Gaia proper motion differences is 2.64 for four measurements. The χ^2 of RV is 146.80 for 150 measurements.

correlation between transiting planet orbital periods and Gaia differential velocities, with short planet periods occurring preferentially with more massive and closer companions. Additionally, our findings suggest a possible trend of shorter planet periods in binaries, although this could be an artifact of the TESS observation bias. If the trend is genuine, it supports the theory that planets in binaries form in smaller protoplanetary disks truncated by their companions.

4. We observe that HCGA high-S/N TOIs exhibit lower differential velocities than the entire population of significant proper motion anomalies stars within 300 pc in the HGCA catalog. This comparison indicates that planets are more likely to persist in systems with low-mass companions or wider stellar companions.

5. We determined the three-dimensional orbit of the companion pair BC around the primary star A in the triple system LTT 1445, which also hosts two transiting planets. Our analysis indicates that LTT 1445 is a flat system, with the orbital plane of BC around A being almost coplanar with the orbital plane of the outer planet

c around B ($\Delta i \sim 2°88$). This coplanarity may account for the survival of multiple planets in an otherwise dynamically challenging environment.

Future observations will provide opportunities to confirm potential companions in systems with no reported companions. Our next paper in the series will feature AO images and astrometric measurements. We will also constrain the companion mass and separation for low-mass companions below the detection limit. Additionally, we will identify the host stars based on transit duration and stellar density and recalculate planet radii by estimating the contrast between the two stars.

Facilities: Kepler, TESS, Gaia, Hipparcos, Keck:I.
Software: orvara (Brandt et al. 2021)

Appendix A
Notes on False Positives in the Target Sample

1. HIP33681 (TOI-510): No obvious NEBs from SG1 but cannot yet clear very close neighbor.
2. HIP15053 (TOI-394): TFOP SG1 identified different odd–even depths in the TESS QLP light curve, which indicates that TOI-394.01 is an EB. The RVs at two quadrature times collected using Keck/HIRES from the primary do not show an RV difference consistent with a stellar mass object. So it is likely that the primary is orbited by a close EB companion and the transit is from the companion pair instead of the primary.
3. HIP21952(TOI-271): TFOP SG1 finds no NEBs.
4. HIP98516 (TOI-1124): TFOP SG1 detected the event on target. But TFOP SG1 also detected strong chromaticity of the transit depth and odd–even depth in the TESS light curve, which indicates TOI-1124.01 is a blend.
5. HIP28122 (TOI-896): TFOP SG1 evaluated it as an FA because of the marginal signal. No transiting events are detected in sector 33, therefore TOI-896.01 retired as an FA.
6. HIP83168 (TOI-1418): TFOP SG1 identified multi-sector data that seem more consistent with stellar variability.
7. HIP58234 (TOI-680): SG1 clears the field of NEBs, and detects a 1ppt event arriving a little early. Additional transits show chromaticity, and HIRES RVs show no convincing variation phased to the ephemeris. This is likely a blend or a planet around the companion.
8. HIP 210000 (TOI-953): TFOP SG1 notes that WASP follow-up RVs show this to be an EB.
9. HIP 22084 (TOI-4314): TOI-4314.01 has a long period of 73 days. TFOP SG1 notes that the transits have low S/Ns and possibly came from stellar variability.
10. HIP 79105 (TOI-2118): TFOP SG1 finds NEB 43″ E.
11. HIP55069 (TOI-1204): No obvious NEB in the SG1 sheet.
12. HIP 70833 (TOI-1946): TOI-1946.01 retired as TFOP FP/NEB.
13. HIP 27844 (TOI-1665): TFOP SG1 finds NEB 32″ E.
14. HIP 67650 (TOI-1837): TFOP SG1 notes that TRES +FIES RVs reveal 33 km s^{-1} variation consistent with a stellar companion.
15. HIP 45621 (TOI-2666): TOI-2666.01 is a single transit. Keck/HIRES spectra show that the star is a spectroscopic binary. The companion is 18.5% the brightness of the secondary and is separated by 35 km s^{-1}.
16. HIP 13754 (TOI-179): TFOP SG1 detects the event on the target
17. HIP 108162 (TOI-1099): TFOP SG1 detects the event on the target.
18. HIP 57386 (TOI-5521): There are no SG1 results available for this system. However, two TRES observations indicate a velocity offset of 29.5 km s^{-1} that is out of phase with the photometric ephemeris. This strongly suggests the presence of a stellar companion in the system, although it cannot be responsible for the shallow transits observed. This is consistent with the WDS catalog, which presents a companion at 0″7 to TOI-5521.
19. HIP 93711 (TOI-2299): Possible on target. SG1 detected the transit, but it is unclear whether it originated from the target or a neighbor at 3″6 to the west. In addition, spoc-s14-s60 detects two Threshold Crossing Events (TCEs) at 214 and 246 days instead of a single TCE at 165 days. But they may not be reliable.
20. HIP 57990 (TOI-635): TFOP SG1 notes that TOI-634, TOI-635, TOI-638 all have similar ephemeris. Possible FA.
21. HIP 65205 (TOI-1831): It is a large star with a close companion at 0°.66. The transit shows a slight odd–even transit depth difference, which could possibly come from an EB. SG1 clears the field of NEBs. But TRES observation does not find a large RV variation, so it retired as an APC/EB?-in SG1. However, as there is a very close companion at 0″66 from the star, it is also possible that the transit event is occurring at the companion, which could explain why large RV variations were not seen in the primary star. We plan to investigate this system further in our project.
22. HIP 24718 (TOI-128): TFOP SG1 finds no NEBs beyond 2″ but they cannot rule out the close companion at ∼2″. If the signal originates from either the primary star or companion, it could still be a planet.
23. HIP 82032 (TOI-909): TFOP SG1 detects an NEB on a nearby, $\Delta T = 6.3$ star, TIC 1310226289. This is consistent with the SPOC centroids.
24. HIP 41849 (TOI-575): TFOP SG1 notes additional TESS data reveal this to be an EB, with primaries and secondaries both visible. Probably on a 0″6 companion seen in high-resolution imaging.
25. HIP 74685 (TOI-2017): TFOP SG1 detects the event on the target. But TOI-2017.01 is an F + M EB with an orbital solution from TRES and the CfA Digital Speedometers.
26. HIP 118045 (TOI-222): TFOP SG1 identified as a spectroscopic eclipsing binary (SEB2).
27. HIP 40694 (TOI-522): TFOP SG1 clears the field of NEBs. HIP 40694 is a rapid rotator, with a *v*sin*i* of 151 km s^{-1}.
28. HIP 54491 (TOI-1799): TFOP SG1 clears the field of NEBs.
29. HIP 78301 (TOI-906): TFOP SG1 detects the event in aperture also containing 1″, $\Delta T = 2.9$ companion.
30. HIP 94780 (K06139): Kepler Eclipsing Binary Catalog v2 (Slawson et al. 2011) marks K06139.01 as an EB.
31. HIP 96501 (K01924): KOI 1924.01 is an FP due to an eclipsing binary 77 mas away.
32. HIP 93954 (K06364): Kepler Eclipsing Binary Catalog v2 (Slawson et al. 2011) marks K06364.01 as an EB.
33. HIP 80474 (EPIC 204165788): Barros et al. (2016) mark it as an eclipsing binary.
34. HIP 54766 (EPIC 201488365): Armstrong et al. (2015) mark it as an eclipsing binary.
35. HIP 41431 (EPIC 212096658): Kruse et al. (2019) mark it as an eclipsing binary.
36. HIP 78977 (EPIC 204506777): Rizzuto et al. (2017) mark it as an eclipsing binary.

Appendix B
LTT 1445 MCMC-fitting Plots
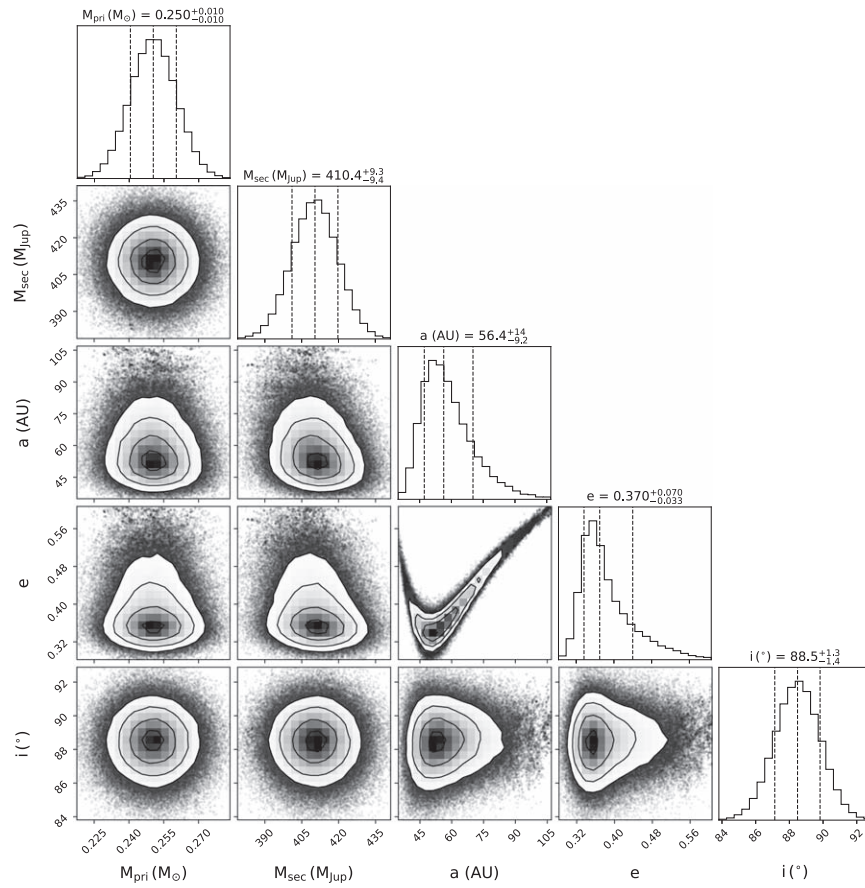
Figure B1. Joint posterior distributions for selected orbital parameters of LTT 1445 BC. These are the host star's mass ($M_{\rm pri}$), the companion mass ($M_{\rm sec}$), the semimajor axis a, the orbital eccentricity e, and the orbital inclination i. The values and histogram distributions of the posteriors of selected parameters are shown, along with 1σ uncertainties.
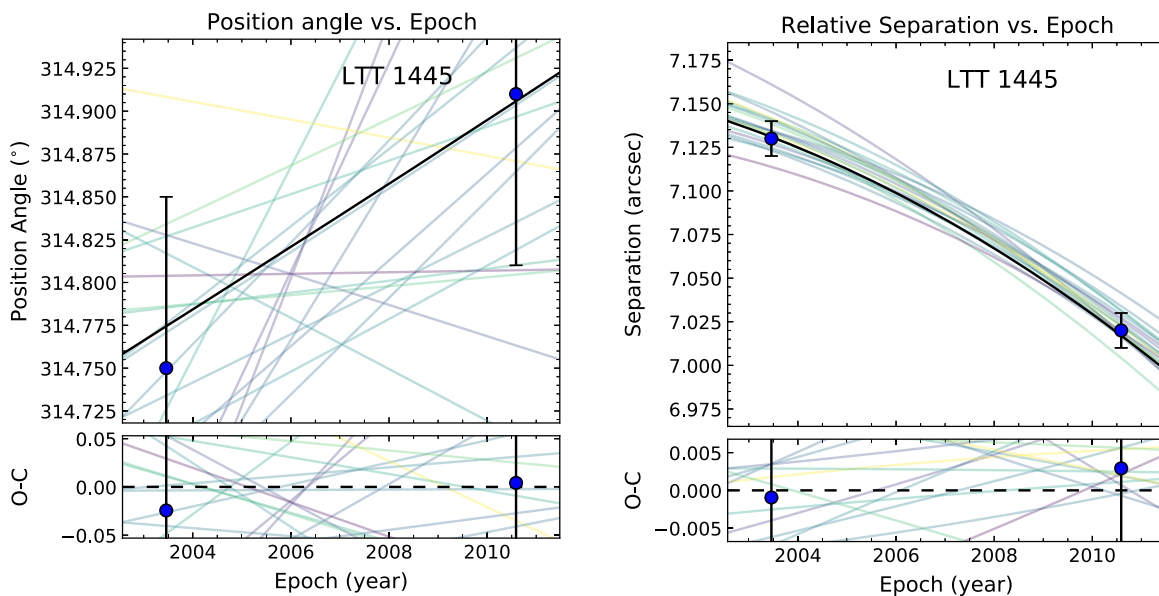
Figure B2. Observed and fitted absolute astrometry for the LTT 1445 system. The two panels show the position angle and relative separation of LTT 1445 BC. The thicker black lines represent the best-fit orbit in the MCMC chain while the other 20 lines represent random draws from the chain.

Appendix C
TOIs with Insignificant Proper Motion Anomalies
(S/N$_G$ < 3) within 300 pc

Table 5
TOIs with Low-S/N Proper Motion Anomalies

Name	HIP Number	P_{pl} days	Exoplanet Archive Disposition[a]	Δv_G m s^{-1}	S/N$_G$	Distance pc
TOI-1011	36964	2.47	PC	3.81	0.47	52.38
TOI-1014	33170	1.41	PC	65.65	1.27	219.9
TOI-1025	46594	9.68	PC	19.66	0.34	130.12
TOI-1028	51271	1.02	FP	4.33	1.18	23.74
TOI-1029	27969	36.22	FP	22.25	2.09	68.69
TOI-1053	95348	5.74	FP	76.28	0.82	266.02
TOI-1054	99212	15.51	CP	14.43	1.02	89.05
TOI-1055	96160	17.47	CP	6.81	0.74	56.79
TOI-1097	61723	9.19	CP	18.23	1.45	79.56
TOI-1097	61723	13.9	CP	18.23	1.45	79.56
TOI-1098	62662	10.18	CP	15.4	0.89	105.14
TOI-1104	91434	341.28	PC	103.48	1.64	68.51
TOI-1127	95774	2.32	FP	35.04	0.8	174.91
TOI-1135	62908	8.03	PC	13.44	0.71	114.18
TOI-1148	52796	5.55	KP	9.68	0.59	96.88
TOI-1150	101252	1.48	KP	16.27	0.42	207.22
TOI-119	31609	5.54	PC	9.89	0.71	66.76
TOI-119	31609	10.69	PC	9.89	0.71	66.76
TOI-120	1419	11.54	CP	19.46	1.53	80.04
TOI-1203	54779	25.52	CP	2.93	0.28	64.96
TOI-1207	37931	2.63	PC	29.16	1.16	113.76
TOI-1233	60689	14.18	CP	12.12	1.37	64.57
TOI-1233	60689	19.59	CP	12.12	1.37	64.57
TOI-1233	60689	6.2	CP	12.12	1.37	64.57
TOI-1233	60689	3.8	CP	12.12	1.37	64.57
TOI-1247	74326	15.92	PC	21.43	1.76	73.39
TOI-1250	88071	1.44	FA	39.3	1.44	66.44
TOI-1255	97166	10.29	CP	11.41	0.97	66.04
TOI-129	65	0.98	CP	42.74	2.43	61.87
TOI-130	3911	14.34	CP	12.34	1.13	57.41
TOI-134	115211	1.4	CP	16.69	1.68	25.18
TOI-1354	102712	1.43	FP	323.06	1.94	248.45
TOI-1355	109028	2.17	PC	34.12	0.82	250.08
TOI-139	110692	11.07	PC	31.29	2.52	42.42
TOI-1407	110758	9.98	KP	14.42	0.77	80.5
TOI-1411	76042	1.45	CP	17.1	2.32	32.46
TOI-1415	71409	14.42	PC	35.65	2.03	111.98
TOI-1416	70705	1.07	PC	9.71	0.85	55.04
TOI-1430	98668	7.43	PC	3.88	0.57	41.24
TOI-1431	104051	2.65	CP	47.14	1.87	149.59
TOI-1434	57350	29.9	PC	9.64	1.52	37.81
TOI-1440	92848	15.52	PC	161.27	1.94	236.48
TOI-1440	92848	4.63	PC	161.27	1.94	236.48
TOI-1462	85268	2.18	CP	6.89	1.46	27.01
TOI-1471	9618	20.77	PC	23.86	1.66	67.29
TOI-1471	9618	683.33	PC	23.86	1.66	67.29
TOI-1475	117382	8.5	PC	32.14	0.75	289.64
TOI-1487	83359	23.29	FA	14.66	0.62	109.73
TOI-1488	85444	0.47	FA	63.85	2.34	159.7
TOI-1514	115710	1.37	FP	123.97	2.77	239.68
TOI-1573	13192	21.22	KP	30.16	2.56	77.43
TOI-1599	11397	1.22	KP	43.04	1.34	121.6
TOI-1608	15767	2.47	APC	3.96	0.15	101.29
TOI-1611	107038	16.2	CP	5.13	1.1	28.28
TOI-1652	61278	0.67	PC	23.65	1.27	129.3
TOI-1682	24323	2.73	KP	14.76	0.72	135.52
TOI-1683	20528	3.06	PC	43.52	2.16	50.94

Table 5
(Continued)

Name	HIP Number	P_{pl} days	Exoplanet Archive Disposition[a]	Δv_G m s^{-1}	S/N$_G$	Distance pc
TOI-1689	84062	9.12	PC	48.89	0.4	28.02
TOI-1718	36272	5.59	PC	8.34	0.82	52.06
TOI-1726	38228	7.11	CP	9.75	2.39	22.38
TOI-1726	38228	20.54	CP	9.75	2.39	22.38
TOI-173	10389	29.75	PC	27.7	1.05	150.07
TOI-174	17264	17.67	CP	1.14	0.14	39.09
TOI-174	17264	29.8	CP	1.14	0.14	39.09
TOI-174	17264	12.16	CP	1.14	0.14	39.09
TOI-174	17264	3.98	CP	1.14	0.14	39.09
TOI-174	17264	7.91	CP	1.14	0.14	39.09
TOI-177	6365	2.85	CP	4.15	0.44	22.45
TOI-1773	43587	0.74	KP	4.35	1.18	12.59
TOI-1774	48443	16.71	CP	10.68	1.02	53.84
TOI-1776	53688	2.8	PC	8.38	0.87	44.75
TOI-1777	49576	14.65	PC	15.73	0.77	80.14
TOI-1778	44746	6.52	PC	41.16	1.64	99.31
TOI-1793	53719	55.09	CP	10.92	1.74	36.97
TOI-180	4460	0.84	APC	159.24	2.21	259.7
TOI-1801	57099	10.64	PC	16.67	1.12	30.89
TOI-1807	65469	0.55	CP	14.14	1.66	42.59
TOI-1821	54906	9.49	KP	1.72	0.42	21.56
TOI-1827	62452	1.47	CP	4.12	1.06	8.08
TOI-1830	73765	9.78	FP	19.35	2.74	50.31
TOI-185	7562	0.94	KP	55.25	2.63	122.79
TOI-186	16069	35.61	CP	2.26	0.51	16.33
TOI-186	16069	7.79	CP	2.26	0.51	16.33
TOI-1860	73869	1.07	CP	5.4	0.74	45.74
TOI-1898	47288	45.52	PC	43.35	2.52	80.13
TOI-193	117883	0.79	CP	12.65	0.8	81.05
TOI-196	4548	1.16	PC	100.38	2.26	290.64
TOI-1969	72490	2.69	FP	45.06	2.28	106.82
TOI-197	116158	14.28	CP	6.35	0.27	95.43
TOI-198	738	10.22	PC	11.5	1.5	23.78
TOI-200	116748	8.14	CP	24.44	2.78	44.18
TOI-2009	5286	nan	PC	13.94	2.42	20.54
TOI-2018	74981	7.44	PC	4.7	0.73	28.04
TOI-2020	80076	5.63	KP	12.17	0.63	128.52
TOI-2024	80838	2.88	KP	9.31	0.77	76.22
TOI-2056	848	10.22	PC	15.34	1.1	92.74
TOI-2069	80243	5.92	PC	10.33	1.74	38.61
TOI-2082	78892	30.2	PC	23.37	2.35	63.74
TOI-2091	86067	177.22	PC	10.72	0.9	70.39
TOI-2105	58868	15.92	PC	33.36	1.84	72.89
TOI-2111	84840	1.27	FP	35.33	2.74	83.16
TOI-2112	113195	14.01	PC	9.16	0.69	86.17
TOI-2112	113195	155.82	PC	9.16	0.69	86.17
TOI-2115	6105	3.69	FP	13.0	0.27	215.64
TOI-2128	83827	16.34	PC	4.49	0.93	36.67
TOI-214	31692	18.55	PC	13.43	1.11	38.94
TOI-214	31692	9.7	PC	13.43	1.11	38.94
TOI-2145	86040	10.26	CP	49.45	1.36	226.24
TOI-2194	98130	15.34	PC	1.97	0.42	19.55
TOI-2211	101503	3.09	PC	3.86	0.19	70.45
TOI-2221	102409	nan	CP	2.48	1.05	9.71
TOI-2259	79876	16.59	PC	39.79	2.09	121.94
TOI-2270	79823	nan	PC	4.37	0.29	94.23
TOI-2301	74576	6.05	PC	23.7	1.28	119.01
TOI-2431	11707	0.22	PC	15.13	1.1	36.01
TOI-2443	12493	15.67	PC	5.98	0.9	23.91
TOI-245	113831	8.77	PC	80.43	2.27	125.06
TOI-2474	24830	4.28	PC	40.22	1.21	132.43
TOI-248	10779	5.99	PC	7.95	0.68	76.09
TOI-253	4468	3.51	PC	3.02	0.32	30.91

Table 5
(Continued)

Name	HIP Number	P_{pl} days	Exoplanet Archive Disposition[a]	Δv_G m s^{-1}	S/N$_G$	Distance pc
TOI-2540	25775	12.72	PC	4.15	0.51	19.16
TOI-2540	25775	22.08	APC	4.15	0.51	19.16
TOI-257	14710	18.39	CP	21.14	1.85	76.86
TOI-260	1532	13.48	PC	4.27	0.88	20.21
TOI-261	4739	3.36	PC	28.81	0.9	113.64
TOI-261	4739	13.04	CP	28.81	0.9	113.64
TOI-262	10117	11.15	CP	3.72	0.43	44.14
TOI-266	8152	10.75	PC	4.92	0.23	101.69
TOI-266	8152	6.19	PC	4.92	0.23	101.69
TOI-282	20295	56.01	CP	16.46	0.74	140.24
TOI-282	20295	31.32	FA	16.46	0.74	140.24
TOI-282	20295	84.26	CP	16.46	0.74	140.24
TOI-282	20295	22.89	CP	16.46	0.74	140.24
TOI-381	7060	4.9	FP	14.48	1.42	75.3
TOI-387	16212	4.16	FP	37.28	0.56	218.8
TOI-389	36612	13.46	FP	20.69	1.16	105.0
TOI-396	13363	5.97	CP	6.67	1.01	31.7
TOI-396	13363	3.59	CP	6.67	1.01	31.7
TOI-396	13363	11.23	CP	6.67	1.01	31.7
TOI-409	33392	6.8	FP	16.24	1.46	53.27
TOI-411	17047	9.57	CP	6.89	0.6	62.9
TOI-411	17047	4.04	CP	6.89	0.6	62.9
TOI-4186	105697	12.76	PC	42.92	2.22	67.61
TOI-4187	14982	30.88	PC	45.53	1.99	154.81
TOI-4189	25359	46.96	PC	6.95	0.63	69.31
TOI-419	33390	0.4	FP	14.45	0.41	42.59
TOI-4191	49531	742.86	PC	19.91	1.06	83.73
TOI-430	18761	0.59	FP	23.17	1.61	66.09
TOI-4302	4599	38.76	PC	82.56	2.61	132.22
TOI-4303	22414	8.61	PC	42.0	0.96	253.4
TOI-4304	41378	15.57	KP	30.64	1.22	105.98
TOI-4304	41378	31.72	KP	30.64	1.22	105.98
TOI-4305	102133	183.0	PC	14.12	0.51	161.04
TOI-4305	102133	374.36	PC	14.12	0.51	161.04
TOI-4307	25351	32.7	PC	1.48	0.31	36.12
TOI-4307	25351	4.65	PC	1.48	0.31	36.12
TOI-4309	51743	87.22	PC	37.57	2.23	76.06
TOI-431	26013	12.46	CP	4.22	0.85	32.62
TOI-431	26013	0.49	CP	4.22	0.85	32.62
TOI-4320	16038	703.62	PC	11.45	0.85	79.43
TOI-4320	16038	46.41	FA	11.45	0.85	79.43
TOI-4321	107911	nan	PC	15.13	0.84	109.32
TOI-4324	47619	6.25	PC	10.41	1.43	17.06
TOI-4326	115828	nan	PC	15.94	1.3	57.77
TOI-4328	21223	703.79	APC	3.9	0.83	25.02
TOI-4330	71815	3.35	PC	138.19	1.76	287.19
TOI-4337	53534	2.29	PC	8.32	0.54	64.83
TOI-4350	10229	4.88	PC	4.93	0.26	103.38
TOI-4355	31179	674.23	PC	19.65	1.62	76.36
TOI-4358	113293	390.46	PC	27.66	2.23	66.28
TOI-4362	34209	7.55	PC	19.13	0.92	134.6
TOI-4369	32099	13.58	PC	197.03	0.25	283.99
TOI-4382	86844	10.69	PC	145.03	2.79	166.34
TOI-440	25670	1.08	FP	12.13	1.33	49.37
TOI-444	19950	17.96	PC	5.34	0.41	57.45
TOI-4470	98505	2.22	KP	6.37	2.58	19.78
TOI-4481	102401	0.93	PC	4.92	1.5	12.06
TOI-4498	96902	5.31	FP	42.77	2.8	79.83
TOI-4517	115752	1.21	KP	25.89	2.84	29.65
TOI-4524	15249	0.93	CP	14.19	1.06	63.86
TOI-4527	6069	0.4	PC	12.56	0.48	18.1
TOI-4537	112100	6.66	PC	35.06	2.66	70.61
TOI-454	15407	18.08	APC	19.11	1.25	79.03

Table 5
(Continued)

Name	HIP Number	P_{pl} days	Exoplanet Archive Disposition[a]	Δv_G m s^{-1}	S/N$_G$	Distance pc
TOI-4580	79180	0.92	PC	2.34	0.24	67.65
TOI-4588	92247	13.12	PC	14.07	0.35	226.82
TOI-4597	22838	4.67	PC	66.83	2.82	124.2
TOI-4599	31635	2.77	CP	1.28	0.49	10.0
TOI-4599	31635	5.71	CP	1.28	0.49	10.0
TOI-4602	18841	3.98	PC	12.48	1.18	62.81
TOI-461	11865	10.92	PC	14.14	1.22	45.74
TOI-4612	29301	4.11	KP	10.87	0.46	134.54
TOI-4626	66854	17.48	PC	12.13	1.21	51.15
TOI-4631	45012	33.64	PC	15.48	1.52	62.26
TOI-4641	13224	22.1	PC	31.72	1.87	87.65
TOI-469	29442	13.63	CP	24.04	2.03	68.0
TOI-480	27849	6.87	PC	22.21	2.84	54.28
TOI-486	31300	1.74	PC	4.28	0.76	15.22
TOI-500	34269	0.55	CP	7.15	0.71	47.41
TOI-5076	15683	23.44	PC	33.03	1.05	82.75
TOI-5082	34271	4.24	PC	10.69	0.98	43.03
TOI-509	38374	9.06	CP	13.6	1.23	48.85
TOI-509	38374	21.4	CP	13.6	1.23	48.85
TOI-5099	13913	14.45	PC	70.32	2.65	91.99
TOI-5108	54186	6.75	PC	67.85	1.48	130.97
TOI-5125	27695	5.91	PC	24.13	0.57	165.4
TOI-5128	46885	7.6	PC	70.07	1.08	192.93
TOI-5141	50496	11.81	KP	48.13	1.68	131.36
TOI-5156	17668	22.85	PC	178.84	1.75	159.46
TOI-5384	51260	2.99	KP	20.02	0.26	218.06
TOI-5387	69858	2.8	PC	22.15	1.03	141.19
TOI-5392	69240	17.53	PC	21.85	2.22	48.51
TOI-5394	50469	15.19	PC	43.9	2.88	64.18
TOI-5401	61637	6.83	PC	137.4	1.4	216.55
TOI-554	18893	7.05	PC	2.83	0.31	45.18
TOI-554	18893	3.04	PC	2.83	0.31	45.18
TOI-560	42401	6.4	CP	10.09	1.36	31.59
TOI-560	42401	18.88	CP	10.09	1.36	31.59
TOI-562	47103	3.93	CP	4.34	1.86	9.44
TOI-5724	80264	697.4	PC	1.9	0.26	50.4
TOI-5739	66730	8.43	PC	19.63	1.87	61.84
TOI-5789	99452	12.93	PC	2.52	0.9	20.44
TOI-5807	101511	14.24	PC	10.79	1.12	73.06
TOI-5809	103502	9.21	PC	229.51	1.73	38.67
TOI-5817	106097	15.61	PC	16.37	1.09	80.34
TOI-5821	104513	2.15	KP	98.31	2.73	182.19
TOI-585	43991	5.55	APC	24.1	0.94	157.55
TOI-587	42654	8.04	PC	37.57	0.96	210.31
TOI-588	33609	39.47	PC	63.0	1.98	151.88
TOI-5951	113300	3.17	PC	65.87	2.72	160.83
TOI-5955	116907	0.59	PC	58.48	1.95	43.07
TOI-5961	114941	1.62	PC	9.09	1.18	26.29
TOI-5972	108859	3.52	KP	7.35	0.7	48.15
TOI-5997	85850	5.66	PC	21.2	2.07	46.62
TOI-6026	74	1.28	PC	8.73	1.2	42.0
TOI-6054	17540	7.49	PC	24.03	1.64	78.73
TOI-6054	17540	12.58	PC	24.03	1.64	78.73
TOI-6075	91906	832.92	PC	7.89	0.84	39.88
TOI-6098	38729	2.73	PC	27.15	2.18	81.72
TOI-651	29118	1.07	PC	30.07	2.03	85.86
TOI-652	48739	3.98	CP	9.51	1.02	45.6
TOI-653	47371	0.69	FP	94.5	1.99	213.86
TOI-664	52733	4.74	KP	10.75	0.48	99.95
TOI-704	28754	3.81	CP	2.78	0.21	29.8
TOI-731	47780	0.32	CP	19.11	1.64	9.42
TOI-740	49678	2.13	PC	21.34	0.87	114.55
TOI-741	45908	7.58	PC	0.46	0.23	10.45

Table 5
(Continued)

Name	HIP Number	P_{pl} days	Exoplanet Archive Disposition[a]	Δv_G m s^{-1}	S/N$_G$	Distance pc
TOI-755	61820	2.54	CP	38.19	1.64	105.82
TOI-801	32674	0.78	PC	21.42	1.73	71.4
TOI-802	31134	3.69	PC	1.31	0.26	28.06
TOI-836	73427	8.6	CP	9.38	1.19	27.51
TOI-836	73427	3.82	PC	9.38	1.19	27.51
TOI-869	16521	26.48	FA	26.0	1.36	110.53
TOI-911	85583	8.58	APC	60.76	2.94	85.17
TOI-957	24689	0.83	FP	39.77	0.64	275.31

Note.
[a] The flags come from the NASA Exoplanet Archive. CP: confirmed planet, PC: planet candidate, APC: ambiguous planet candidate, FP: false positive, FA: false alarm.

(This table is available in its entirety in machine-readable form.)

ORCID iDs

Jingwen Zhang (张婧雯) ⓘ https://orcid.org/0000-0002-2696-2406

Lauren M. Weiss ⓘ https://orcid.org/0000-0002-3725-3058

Daniel Huber ⓘ https://orcid.org/0000-0001-8832-4488

Eric L. N. Jensen ⓘ https://orcid.org/0000-0002-4625-7333

Timothy D. Brandt ⓘ https://orcid.org/0000-0003-2630-8073

Karen Collins ⓘ https://orcid.org/0000-0001-6588-9574

Dennis M. Conti ⓘ https://orcid.org/0000-0003-2239-0567

Howard Isaacson ⓘ https://orcid.org/0000-0002-0531-1073

Pablo Lewin ⓘ https://orcid.org/0000-0003-0828-6368

Giuseppe Marino ⓘ https://orcid.org/0000-0001-8134-0389

Bob Massey ⓘ https://orcid.org/0000-0001-8879-7138

Felipe Murgas ⓘ https://orcid.org/0000-0001-9087-1245

Enric Palle ⓘ https://orcid.org/0000-0003-0987-1593

Don J. Radford ⓘ https://orcid.org/0000-0002-3940-2360

Chris Stockdale ⓘ https://orcid.org/0000-0003-2163-1437

Thiam-Guan Tan ⓘ https://orcid.org/0000-0001-5603-6895

Gavin Wang ⓘ https://orcid.org/0000-0003-3092-4418

References

Adams, F. C., Ruden, S. P., & Shu, F. H. 1989, ApJ, 347, 959
Akeson, R. L., Chen, X., Ciardi, D., et al. 2013, PASP, 125, 989
Akeson, R. L., Jensen, E. L. N., Carpenter, J., et al. 2019, ApJ, 872, 158
Armstrong, D. J., Kirk, J., Lam, K. W. F., et al. 2015, A&A, 579, A19
Artymowicz, P., & Lubow, S. H. 1994, ApJ, 421, 651
Badenas-Agusti, M., Günther, M. N., Daylan, T., et al. 2020, AJ, 160, 113
Barros, S. C. C., Demangeon, O., & Deleuil, M. 2016, A&A, 594, A100
Batalha, N. M., Rowe, J. F., Bryson, S. T., et al. 2013, ApJS, 204, 24
Borucki, W. J., Koch, D., Basri, G., et al. 2010, Sci, 327, 977
Brandt, T. D. 2021, ApJS, 254, 42
Brandt, T. D., Dupuy, T. J., & Bowler, B. P. 2019, AJ, 158, 140
Brandt, T. D., Dupuy, T. J., Li, Y., et al. 2021, AJ, 162, 186
Burke, C. J., Bryson, S. T., Mullally, F., et al. 2014, ApJS, 210, 19
Cadman, J., Hall, C., Fontanive, C., & Rice, K. 2022, MNRAS, 511, 457
Campante, T. L., Barclay, T., Swift, J. J., et al. 2015, ApJ, 799, 170
Correia, A. C. M., Udry, S., Mayor, M., et al. 2008, A&A, 479, 271
Coughlin, J. L., Mullally, F., Thompson, S. E., et al. 2016, ApJS, 224, 12
Cox, E. G., Harris, R. J., Looney, L. W., et al. 2017, ApJ, 851, 83
Cumming, A., Butler, R. P., Marcy, G. W., et al. 2008, PASP, 120, 531
Damasso, M., Sozzetti, A., Lovis, C., et al. 2020, A&A, 642, A31
De Rosa, R. J., Dawson, R., & Nielsen, E. L. 2020, A&A, 640, A73
Dieterich, S. B., Henry, T. J., Golimowski, D. A., Krist, J. E., & Tanner, A. M. 2012, AJ, 144, 64
Dumusque, X., Turner, O., Dorn, C., et al. 2019, A&A, 627, A43
Dupuy, T. J., Kratter, K. M., Kraus, A. L., et al. 2016, ApJ, 817, 80
Dupuy, T. J., Kraus, A. L., Kratter, K. M., et al. 2022, MNRAS, 512, 648

ESA 1997, ESA SP-1200, The Hipparcos and Tycho Catalogues (Noordwijk: ESA)
Fontanive, C., & Bardalez Gagliuffi, D. 2021, FrASS, 8, 16
Fulton, B. J., Rosenthal, L. J., Hirsch, L. A., et al. 2021, ApJS, 255, 14
Furlan, E., Ciardi, D. R., Everett, M. E., et al. 2017, AJ, 153, 71
Gaia Collaboration, Klioner, S. A., Lindegren, L., et al. 2022, A&A, 667, A148
Gandolfi, D., Barragán, O., Livingston, J. H., et al. 2018, A&A, 619, L10
Gandolfi, D., Fossati, L., Livingston, J. H., et al. 2019, ApJL, 876, L24
Guerrero, N. M., Seager, S., Huang, C. X., et al. 2021, ApJS, 254, 39
Hatzes, A. P., Cochran, W. D., Endl, M., et al. 2003, ApJ, 599, 1383
Hatzes, A. P., Gandolfi, D., Korth, J., et al. 2022, AJ, 163, 223
Hirsch, L. A., Rosenthal, L., Fulton, B. J., et al. 2021, AJ, 161, 134
Hobson, M. J., Brahm, R., Jordán, A., et al. 2021, AJ, 161, 235
Howard, A. W., Marcy, G. W., Bryson, S. T., et al. 2012, ApJS, 201, 15
Howell, S. B., Matson, R. A., Ciardi, D. R., et al. 2021, AJ, 161, 164
Howell, S. B., Sobeck, C., Haas, M., et al. 2014, PASP, 126, 398
Huber, D., Bryson, S. T., Haas, M. R., et al. 2016, ApJS, 224, 2
Huber, D., Carter, J. A., Barbieri, M., et al. 2013, Sci, 342, 331
Jang-Condell, H., et al. 2015, ApJ, 799, 147
Jones, H. R. A., Paul Butler, R., Tinney, C. G., et al. 2002, MNRAS, 333, 871
Kane, S. R., Barclay, T., Hartmann, M., et al. 2015, ApJ, 815, 32
Kervella, P., Arenou, F., Mignard, F., & Thévenin, F. 2019, A&A, 623, A72
Kostov, V. B., Mullally, S. E., Quintana, E. V., et al. 2019, AJ, 157, 124
Kozai, Y. 1962, AJ, 67, 591
Kraus, A. L., Ireland, M. J., Huber, D., Mann, A. W., & Dupuy, T. J. 2016, AJ, 152, 8
Kruse, E., Agol, E., Luger, R., & Foreman-Mackey, D. 2019, ApJS, 244, 11
Lavie, B., Bouchy, F., Lovis, C., et al. 2023, A&A, 673, A69
Lester, K. V., Matson, R. A., Howell, S. B., et al. 2021, AJ, 162, 75
Lidov, M. L. 1962, P&SS, 9, 719
Lindegren, L., Hernández, J., Bombrun, A., et al. 2018, A&A, 616, A2
Lubin, J., Van Zandt, J., Holcomb, R., et al. 2022, AJ, 163, 101
Luyten, W. J. 1957, A Catalogue of 9867 Stars in the Southern Hemisphere with Proper Motions Exceeding 0."2 Annually (Minneapolis, MN: Lund Press)
Luyten, W. J. 1980, NLTT Catalogue, Volume_III, 0_ to −30_ (Mineapolis, MN: Univ. Minnesota)
Manara, C. F., Tazzari, M., Long, F., et al. 2019, A&A, 628, A95
Mason, B. D., Wycoff, G. L., Hartkopf, W. I., Douglass, G. G., & Worley, C. E. 2001, AJ, 122, 3466
Mills, S. M., & Fabrycky, D. C. 2017, ApJL, 838, L11
Moe, M., & Kratter, K. M. 2018, ApJ, 854, 44
Moe, M., & Kratter, K. M. 2021, MNRAS, 507, 3593
Mullally, F., Coughlin, J. L., Thompson, S. E., et al. 2015, ApJS, 217, 31
Offner, S. S. R., Moe, M., Kratter, K. M., et al. 2023, in ASP Conf. Ser. 534, Protostars and Planets VII (San Francisco, CA: ASP), 275
Orell-Miquel, J., Nowak, G., Murgas, F., et al. 2023, A&A, 669, A40
Paczynski, B. 1977, ApJ, 216, 822
Perryman, M. A. C., Lindegren, L., Kovalevsky, J., et al. 1997, A&A, 323, L49
Pichardo, B., Sparke, L. S., & Aguilar, L. A. 2005, MNRAS, 359, 521
Pope, B. J. S., Parviainen, H., & Aigrain, S. 2016, MNRAS, 461, 3399
Quintana, E. V., Adams, F. C., Lissauer, J. J., & Chambers, J. E. 2007, ApJ, 660, 807

Raghavan, D., McAlister, H. A., Henry, T. J., et al. 2010, ApJS, 190, 1

Ricker, G. R., Winn, J. N., Vanderspek, R., et al. 2014, Proc. SPIE, 9143, 914320

Rizzuto, A. C., Mann, A. W., Vanderburg, A., Kraus, A. L., & Covey, K. R. 2017, AJ, 154, 224

Rodriguez, D. R., Duchêne, G., Tom, H., et al. 2015, MNRAS, 449, 3160

Rossiter, R. A. 1955, POMic, 11, 1

Rowe, J. F., Coughlin, J. L., Antoci, V., et al. 2015, ApJS, 217, 16

Rudak, B., & Paczynski, B. 1981, AcA, 31, 13

Simpson, A., & Cloutier, R. 2022, AAS Meeting Abstracts, 54, 403.10

Slawson, R. W., Prša, A., Welsh, W. F., et al. 2011, AJ, 142, 160

Sullivan, K., Kraus, A. L., Huber, D., et al. 2023, AJ, 165, 177

Teske, J. K., Ciardi, D. R., Howell, S. B., Hirsch, L. A., & Johnson, R. A. 2018, AJ, 156, 292

Thompson, S. E., Coughlin, J. L., Hoffman, K., et al. 2018, ApJS, 235, 38

Trifonov, T., Tal-Or, L., Zechmeister, M., et al. 2020, A&A, 636, A74

Wang, J., Fischer, D. A., Xie, J.-W., & Ciardi, D. R. 2015, ApJ, 813, 130

Winters, Jennifer G., Cloutier, Ryan, Medina, Amber A., et al. 2022, AJ, 163, 168

Winters, J. G., Medina, A. A., Irwin, J. M., et al. 2019, AJ, 158, 152

Xuan, J. W., & Wyatt, M. C. 2020, MNRAS, 497, 2096

Zagaria, F., Rosotti, G. P., Alexander, R. D., & Clarke, C. J. 2023, EPJP, 138, 25

Zanazzi, J. J., & Lai, D. 2018, MNRAS, 477, 5207

Zhang, J., Weiss, L. M., Huber, D., et al. 2021, AJ, 162, 89

Zhang, Z., Bowler, B. P., Dupuy, T. J., et al. 2023, AJ, 165, 73

Zhou, G., Wirth, C. P., Huang, C. X., et al. 2022, AJ, 163, 289

Ziegler, C., Tokovinin, A., Briceño, C., et al. 2020, AJ, 159, 19

Ziegler, C., Tokovinin, A., Latiolais, M., et al. 2021, AJ, 162, 192

Zink, J. K., Hardegree-Ullman, K. K., Christiansen, J. L., et al. 2021, AJ, 162, 259

Zurlo, A., Cieza, L. A., Pérez, S., et al. 2020, MNRAS, 496, 5089